PHILOSOPHICAL TRANSACTIONS OF THE ROYAL SOCIETY A MATHEMATICAL, PHYSICAL & ENGINEERING SCIENCES

A Linear Stratified Ocean Model of the Coastal Undercurrent

J. P. McCreary

Phil. Trans. R. Soc. Lond. A 1981 **302**, 385-413
doi: 10.1098/rsta.1981.0176

Phil. Trans. R. Soc. Lond. A. **302**, 385–413 (1981) [385]
Printed in Great Britain

A LINEAR STRATIFIED OCEAN MODEL OF THE COASTAL UNDERCURRENT

By J. P. McCreary, Jr
Oceanographic Center, Nova University, 8000 N. Ocean Drive, Dania, Florida 33004, U.S.A.

(*Communicated by Sir James Lighthill, F.R.S. – Received 16 December 1980*)

CONTENTS

PAGE

1. Introduction 386
   (*a*) Observational background 386
   (*b*) Theoretical background 388
   (*c*) The present approach 389
2. The model ocean 390
3. The solution 392
4. Results 395
   (*a*) The model Undercurrent 397
   (*b*) The dependence on model parameters 397
   (*c*) The *f*-plane response 401
5. Dynamics 403
   (*a*) Simpler models 403
   (*b*) The present model 406
6. Summary and discussion 408

Appendix 409

References 412

The linear, stratified ocean model of McCreary (1981) is used to study the wind-driven response of the ocean near an eastern coast. The model can be regarded as an extension of the inviscid models of Lighthill (1969) and of Gill & Clarke (1974) that allows the vertical diffusion of heat and momentum into the deep ocean. Solutions are still found as expansions of vertical normal modes. Vertical mixing affects each mode as a linear drag with a drag coefficient that increases rapidly with mode-number, n.

A zonally uniform band of steady equatorward winds forces the ocean, and the resulting flow field has many features in common with observations at eastern boundaries. There is a surface equatorward jet and a poleward Coastal Undercurrent confined within 10–20 km of the coast. Both currents extend well poleward of the wind band. Upwelling does not reach great depths, but occurs only above the core of the Undercurrent. Weak downwelling occurs at greater depths. There is offshore Ekman drift in the surface mixed layer and return flow at a depth slightly above the core of the Undercurrent.

The baroclinic alongshore pressure gradient field and the vertical mixing of heat and momentum are essential elements of the model dynamics, but the β-effect and horizontal

mixing are not. Low-order vertical modes ($n < 6$) tend to adjust to Sverdrup balance by the radiation of Kelvin and Rossby waves. These modes establish the alongshore pressure gradient field. High-order modes ($n > 6$) tend toward a two-dimensional balance. They generate the transverse circulation pattern associated with coastal Ekman pumping.

1. Introduction

Subsurface poleward currents are a common feature of oceanic circulation near eastern ocean boundaries (Wooster & Reid 1963). Historically, their existence has been inferred from maps of dynamic topography, with the aid of the geostrophic approximation, and from patterns of water mass characteristics. These studies suggested that the strength of the currents decays away from the coast, and also that weak poleward flow extends a considerable distance offshore. Recently, direct current measurements have shown that strong poleward flow occurs as a very narrow coastal jet: the Coastal Undercurrent. The presence of this jet is especially puzzling because the prevailing winds that presumably drive the flow are equatorward. There are many papers dealing with the phenomenon, and no attempt will be made here to review all of the relevant literature. More detailed introductions to the pertinent observations can be found in Mittelstadt *et al.* (1975), Hickey (1979) and Brockmann *et al.* (1980). Various models of coastal circulation, including models of the Coastal Undercurrent, are reviewed extensively by O'Brien *et al.* (1977) and Allen (1980).

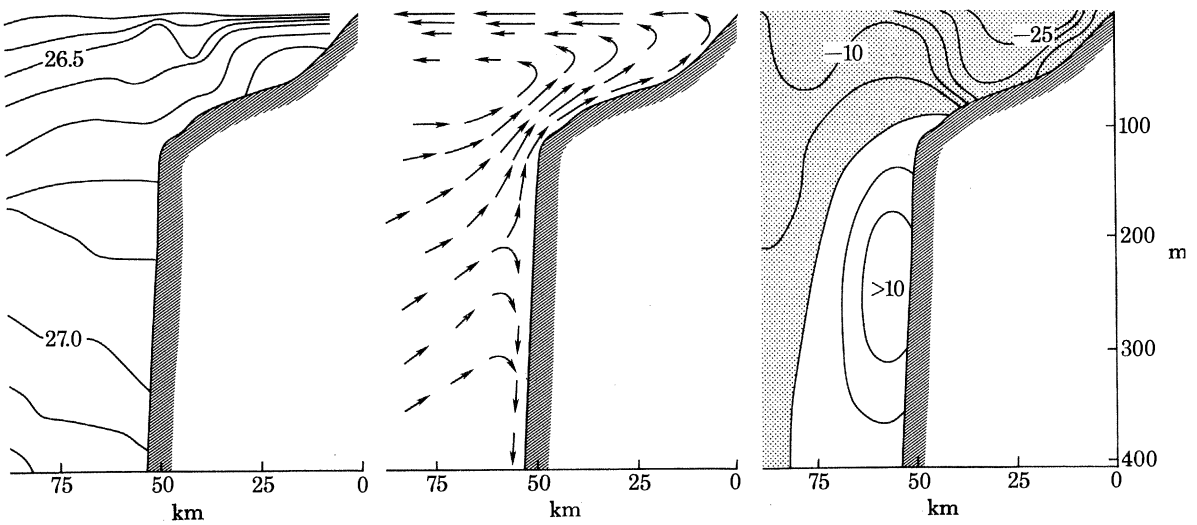

Figure 1. An example of the Northwest African Undercurrent at 21° 40′ N in February–April 1974. The left-hand panel shows profiles of σ_t during a time of weak winds. The contour interval is 0.1. The middle panel is a schematic diagram of the transverse circulation typically observed during the experiment. The right-hand panel shows contours of the mean alongshore current. The contour interval is 5 cm/s. The shaded region indicates southward flow. After Mittelstadt *et al.* (1975) and Huyer (1976).

(a) *Observational background*

Figure 1, adapted from Mittelstadt *et al.* (1975) and Huyer (1976), shows an example of the Coastal Undercurrent off the western coast of North Africa in February–April 1974. During this time the mean equatorward wind stress was 1–2 dyn/cm².† The poleward current is roughly

† dyn = 10^{-5} N.

20 km wide, extends from 100 m to a depth greater than 400 m, and reaches a maximum speed greater than 10 cm/s at a depth of about 250 m. Surface equatorward flow extends over the shelf and reaches speeds in excess of 25 cm/s. Above the current core, isopycnals slope upwards toward the coast, whereas beneath the core they slope downwards. This isopycnal distribution is consistent with that of a geostrophically balanced Undercurrent. The figure also illustrates schematically the typical transverse circulation pattern that was observed during the experiment. On the shelf there is a strong offshore surface drift and near-bottom return flow with mean speeds of the order of 10 cm/s. Strongest upwelling takes place at the shelf break, and estimates of vertical velocity often exceed 0.01 cm/s there. There is weak downwelling at greater depths along the continental slope.

There is considerable evidence that a flow field like that of figure 1 is closely coupled to the alongshore component of the local wind stress, τ^y. For example, off Northwest Africa all current fluctuations are highly correlated with changes in τ^y. Off Oregon and Peru the onshore–offshore flow, and therefore the upwelling circulation, is correlated with τ^y, but the alongshore flow very often is not (Huyer 1976; Brink *et al.* 1978). These observations suggest that the transverse circulation is primarily locally forced by τ^y, but that the alongshore flow is both locally and remotely forced.

The California Undercurrent occurs in conjunction with a baroclinic pressure gradient field that weakens rapidly with depth. Reid & Mantyla (1976) show the mean dynamic height of the sea surface along the west coast of North America. Sea level drops 12 dyn cm (referenced to 500 dB) from 25° to 38° N. This drop corresponds to a sea surface slope somewhat greater than -8×10^{-8} and is equivalent to a poleward pressure gradient force ($-\rho_0^{-1}p_y$) of 8×10^{-5} dyn/g. Sea level rises 3 dyn cm from 38° to 49° N, equivalent to an equatorward pressure gradient force of about -2.5×10^{-5} dyn/g. Wyllie (1966) and Chelton (1980) present monthly maps of the dynamic topography of the sea surface and the 200 dB surface off California and Baja California. In the autumn sea level drops roughly 16 dyn cm from 25° to 38° N; in the spring the drop reduces to 8 dyn cm. The annual mean is about 12 dyn cm, in agreement with Reid & Mantyla (1976). The dynamic topography at 200 dB is much more level. In the autumn this surface drops 4 dyn cm from 25° to 38° N, whereas in the spring there is no decrease at all.

Similar baroclinic pressure fields are apparently associated with other coastal undercurrents as well. Mittelstadt (1978) reports that subsurface isopycnals slope upward from 10° to 30° N along the coast of Northwest Africa. For example, in late winter of 1973 the isopycnal, $\sigma_t = 26.8$, rose from 300 m at 10° N to 100 m at 30° N. On the assumption of a level of no motion at greater depths, the near-surface dynamic height field must slope downwards toward the north. In fact, according to Defant (1941), sea level typically does decrease poleward by 22 dyn cm in that region. Similarly, Brink *et al.* (1978) note a southward rise of subsurface isotherms off the coast of Peru, and conclude that there must be a near-surface poleward pressure gradient.

Vertical mixing processes may play an important role in the dynamics of the Coastal Undercurrent. Wooster & Jones (1970) describe the water mass characteristics of a remarkably strong example of the California Undercurrent where the flow reached a maximum speed of 40 cm/s. In contrast to the water farther offshore, the water of the jet consisted of numerous relatively homogeneous layers 4–25 m thick. In addition, there were several instances of density inversions, and the average value of the Richardson number was very low. All of these properties are indicative of intense vertical mixing.

There may be a tendency for the Coastal Undercurrent to deepen and weaken toward the

PHILOSOPHICAL TRANSACTIONS OF THE ROYAL SOCIETY A MATHEMATICAL, PHYSICAL & ENGINEERING SCIENCES

poles. According to Mittelstadt (1978), the Northwest African Undercurrent occurs at a depth of 100–200 m south of 20° N and then deepens rapidly farther to the north. North of 30° N poleward flow is only marginally perceptible at depths between 500 and 1000 m. Wooster & Gilmartin (1961) show a salinity section taken 100 miles off the coast of South America and extending from the equator to 40° S. A high salinity tongue beginning roughly at 15° S indicates the presence of the Peru–Chile Undercurrent. At 15° S the tongue occurs at a depth of 100 m, whereas at 35° S it occurs at 300 m.

(*b*) *Theoretical background*

The observations suggest that stratification, the establishment of a baroclinic alongshore pressure gradient field, and the vertical mixing of heat and momentum are all involved in the dynamics of the Coastal Undercurrent. Theory also indicates the importance of these processes in that solutions of models lacking one or more of them have unrealistic features. For example, the flow fields of unstratified ocean models are not surface-trapped, but extend to the ocean bottom; moreover, their dynamics necessarily involve horizontal mixing (Pedlosky 1968; Durance & Johnson 1970; Garvine 1971). Two-dimensional, stratified models with no vertical mixing cannot reach a steady state (Charney 1955; Yoshida 1955; O'Brien & Hurlburt 1972). Two-dimensional, stratified models that include vertical mixing can produce a sensible flow field if they are applied to a layer 100–200 m thick (Allen 1973), but if they are applied to the entire water column they generate unrealistically large currents (see the discussion of figure 9). Three-dimensional, inviscid models that include the β-effect, that is, the variation of the Coriolis parameter with latitude, produce no coastal currents at all (Anderson & Gill 1975; also see the discussion of figures 10 and 11). Other models that neglect the vertical mixing of momentum but not of heat are subject to troublesome singularities in the upwelling corner (Pedlosky 1969).

Yoshida (1967) first studied the coastal wind-driven response of an ocean model that was three-dimensional, viscid and stratified. The model consisted of two responsive homogeneous layers, situated above an inert deeper ocean (that is, pressure gradients in the deep ocean were assumed zero). The equilibrium depth of the interface between layers was set to 100 m, to represent the strong near-surface pycnocline characteristic of the coastal ocean. The depth of the lower layer was set to 1000 m, the approximate lower limit of significant ocean currents in the region. Vertical mixing of heat and momentum took the form of very simple drag laws. The mixing of heat was assumed to be proportional to h, the departure of the layer interface from its equilibrium position, and the mixing of momentum was taken to be proportional to the velocity difference between the layers.

Yoshida described the response of his model (see the discussion of figure 12) to a wind band like that of figure 3. Outside the coastal zone the wind drives an offshore Ekman drift in the upper layer, and there is a compensating return flow in the lower layer. Within the coastal zone (of width closely related to the internal Rossby radius of deformation) the interface bends up sharply toward the coast, and the rise extends considerably poleward of the region of the wind band. Associated with this interfacial displacement is a baroclinic pressure field, and at the coast there is a poleward pressure gradient in the region of the wind band. There are strong, coastal geostrophic alongshore currents; the upper layer current is equatorwards, and the lower layer flow is poleward. The upwelling of fluid between layers is proportional to h, and so strong coastal upwelling occurs in the region of the wind band and considerably polewards as well. All of these features of the solution compare well with the observations.

PHILOSOPHICAL TRANSACTIONS OF THE ROYAL SOCIETY A MATHEMATICAL, PHYSICAL & ENGINEERING SCIENCES

In spite of its successes, the Yoshida model has two unavoidable drawbacks. First, the equilibrium thickness of each layer must be set by external assumptions. As a result, the depth scales of the model are adjusted arbitrarily. In a complete theory of the Coastal Undercurrent, the depth scales of the flow field must emerge internally as a result of the solution of the equations of motion. Second, the description of vertical mixing in the ocean as simple drag is both uncommon and not very realistic. There is no sensible way to select values for drag coefficients.

Pedlosky (1974) studied a continuously stratified ocean model that did generate its own depth scales. The model also allowed horizontal and vertical mixing of heat and momentum in the familiar diffusive form. Pedlosky solved the equations of motion in a closed ocean basin and for an arbitrary wind stress distribution. He did not find an exact solution, but rather described the model response to a uniform wind in a cylindrical basin. The most important property of the response is that for sufficiently small alongshore scales of the wind field the flow no longer extends throughout the water column but is confined near the ocean surface. In addition, over much of the basin perimeter the near-surface alongshore current flows against the wind. The surface trapping is closely associated with the establishment of an alongshore baroclinic pressure gradient field that tends to balance the alongshore component of the wind.

McCreary (1981) studied a continuously stratified model with diffusive mixing that also generates a surface-trapped flow field. The model was forced by an equatorial patch of westward wind, similar to the trade-wind field in the Pacific Ocean, and it developed a realistic equatorial current structure. Just beneath the westward surface drift there is an eastward-flowing Equatorial Undercurrent with width, thickness, and magnitude that compare favourably with those observed. In the region of the wind there is a strong divergence of surface water from the equator, convergence of fluid at the core of the Undercurrent, and weaker downwelling below. Again, the surface trapping of the current is closely related to the structure of the baroclinic pressure field. This structure is set up by the radiation of equatorially trapped Rossby and Kelvin waves.

(*c*) *The present approach*

This paper continues the effort to relate the Coastal Undercurrent to the presence of equatorward winds. The model is essentially the equatorial model of McCreary (1981) applied to the coastal ocean. In order that solutions can be represented as sums of vertical normal modes, vertical diffusion coefficients and boundary conditions are restricted to specific forms. Another assumption is that the alongshore flow field is in geostrophic balance. It is possible to include horizontal mixing in the dynamics of the model, and the effects of this process on the Coastal Undercurrent are discussed in the Appendix.

The model is similar to several previous ones. It can be regarded as an extension of the inviscid models of Lighthill (1969) and of Gill & Clarke (1974) that allows the vertical mixing of heat and momentum in the deep ocean. It can also be regarded as a generalization of the two-layer model of Yoshida (1967) to a continuously stratified ocean. Finally, the dynamics of the model are closely related to the model of Pedlosky (1974). Similarities to these earlier studies are noted at several points.

The model is able to account for many of the observed features of the coastal flow field. In particular, there is a narrow Coastal Undercurrent driven by equatorward winds that has its current maximum only 100–300 m below the ocean surface. As expected, a baroclinic alongshore pressure gradient field and the vertical mixing of heat and momentum are both necessary for the existence of a realistic Coastal Undercurrent; however, the β-effect and horizontal mixing are

not. As in the McCreary (1981) model the alongshore pressure gradient field is established by the radiation of Kelvin and Rossby waves.

2. The model ocean

In a state of no motion the model ocean has a stably stratified background density structure $\rho_b(z)$ and associated Väisälä frequency $N_b(z)$. The equations of motion, linearized about this background state, are

$$\left.\begin{aligned} u_t - fv + p_x &= (\nu u_z)_z + \nu_h \nabla^2 u, \\ v_t + fu + p_y &= (\nu v_z)_z + \nu_h \nabla^2 v, \\ u_x + v_y + w_z &= 0, \\ \rho_t - (1/g)\, N_b^2 w &= (\kappa\rho)_{zz} + \kappa_h \nabla^2 \rho, \\ p_z &= -\rho g, \end{aligned}\right\} \tag{1}$$

where the coefficients of vertical eddy viscosity and diffusivity are given by

$$\nu = A/N_b^2, \quad \kappa = (1/\sigma)\,(A/N_b^2), \tag{2}$$

in which $\sigma = \nu/\kappa$ is the Prandtl number. Coefficients of horizontal eddy viscosity and diffusivity are ν_h and κ_h respectively. The zonal, meridional and vertical velocity fields are u, v and w, respectively; p and ρ are the pressure and density changes from the background state; f is the Coriolis parameter; and g is the acceleration due to gravity. Constant factors of $\bar{\rho}$, the average density of the water column, are everywhere ignored. The x-axis is oriented eastward and the y-axis is oriented northward with its origin at the equator. A comprehensive discussion of linearized sets of equations similar to (1) can be found in Veronis (1973) or Moore & Philander (1978).

The vertical mixing terms are unconventional. First, mixing coefficients are assumed to be inversely proportional to the square of the Väisälä frequency. Second, the vertical diffusion of heat and momentum have slightly different forms. Both of these choices are crucial to the method of solution adopted here. Only in this way is it possible to find solutions as expansions of vertical normal modes. Other workers have already recognized the mathematical convenience of these forms of vertical mixing; Fjeldstad (1963), and later Mork (1972), used them in their internal wave studies.

Although the choices of vertical mixing coefficients are made for mathematical convenience, they are sensible for dynamical reasons. Equations (2) express the intuitive idea that wherever background stratification is strong, vertical mixing is weak. Turner (1973), in his discussion of turbulence, considers vertical mixing processes of this form. More recently, Lilly *et al.* (1974) and Caldwell *et al.* (1980) have found the relation useful in their studies of atmospheric and oceanic turbulence.

Surface boundary conditions, at $z = 0$, are

$$\nu u_z = \tau^x, \quad \nu v_z = \tau^y, \quad w = \kappa\rho = 0, \tag{3}$$

where τ^x and τ^y are the zonal and meridional components of the wind stress at the ocean surface. The ocean bottom, at $z = -D$, is assumed flat. Boundary conditions there are

$$\nu u_z = \nu v_z = w = \kappa\rho = 0. \tag{4}$$

If $N_b(z)$ changes discontinuously at some level in the water column, $z = -H$, then equations (1) require that

$$u, v, p, w, \rho, \nu u_z, \nu v_z, (\kappa\rho)_z \quad \text{are continuous} \tag{5}$$

across the interface.

The choices of boundary conditions (3)–(5) are also necessary to be able to find solutions as expansions of vertical normal modes. Two of the conditions are not very realistic. The condition that stress, rather than velocity, is zero at the ocean bottom means that the bottom is very slippery, and therefore that a significant bottom Ekman layer is not possible. In fact, the lack of a bottom Ekman layer is not serious. It would be worrisome only if solutions developed large bottom currents, and, provided that the model includes the β-effect, currents are always strongly surface-trapped (see the discussion of equation (31)). The requirement that ρ, rather than the heat flux, is zero at the ocean surface fixes the temperature there, and so the model cannot generate any sea surface temperature variations. This condition is not defendable since an important aspect of the observed response of the coastal ocean to equatorward winds is the appearance of cold upwelled water at the ocean surface. Nevertheless, this condition is mathematically so convenient that it has been commonly used (Pedlosky 1969; Allen 1973; Pedlosky 1974).

Solutions to (1), subject to the boundary conditions (3)–(5), can be expressed in terms of the eigenfunctions, ψ_n, that satisfy

$$\psi_{nz} = -\frac{N_b^2}{c_n^2}\int_{-D}^{z}\psi_n\,dz, \tag{6}$$

subject to

$$\frac{1}{c_n^2}\int_{-D}^{0}\psi_n\,dz = 0. \tag{7}$$

If there is a discontinuity in $N_b(z)$, at $z = -H$, (6) is solved so that

$$\psi_n(z) \quad \text{is continuous} \tag{8}$$

across the interface. The eigenfunctions are commonly normalized so that

$$\psi_n(0) = 1. \tag{9}$$

Finally, it is convenient to order them so that the eigenvalues c_n decrease monotonically. In that case as $n \to \infty$, $c_n \to$ const. $\times (1/n)$. The $n = 0$ mode is unique in that $c_0 = \infty$; this mode is the barotropic mode of the system. The remaining modes have finite values of c_n; they form an infinite set of baroclinic modes.

The solutions are then given by

$$\left.\begin{aligned} u = \sum_{n=1}^{N} u_n\psi_n, \quad v = \sum_{n=1}^{N} v_n\psi_n, \quad p = \sum_{n=1}^{N} p_n\psi_n, \\ w = \sum_{n=1}^{N} w_n\int_{-D}^{z}\psi_n\,dz, \quad \rho = \sum_{n=1}^{N}\rho_n\psi_{nz}, \end{aligned}\right\} \tag{10}$$

where the expansion coefficients are functions only of x, y and t. The equations governing the expansion coefficients are

$$\left.\begin{aligned} (\partial_t + \omega_n)\,u_n - fv_n + p_{nx} &= F_n + \nu_h\nabla^2 u_n, \\ (\partial_t + \omega_n)\,v_n + fu_n + p_{ny} &= G_n + \nu_h\nabla^2 v_n, \\ \left(\partial_t + \frac{\omega_n}{\sigma}\right)\frac{p_n}{c_n^2} + u_{nx} + v_{ny} &= \frac{\kappa_h}{c_n^2}\nabla^2 p_n, \\ w_n = \left(\partial_t + \frac{\omega_n}{\sigma} + \kappa_h\nabla^2\right)\frac{p_n}{c_n^2}, \quad \rho_n &= -\frac{p_n}{g}, \end{aligned}\right\} \tag{11}$$

where

$$\omega_n = A/c_n^2. \tag{12}$$

The coupling coefficients of each mode to the wind field are

$$F_n = \tau^x \Big/ \int_{-D}^{0} \psi_n^2 \, \mathrm{d}z, \quad G_n = \tau^y \Big/ \int_{-D}^{0} \psi_n^2 \, \mathrm{d}z. \tag{13}$$

The first three equations of (11) are solved for the three unknowns u_n, v_n and p_n. The last two equations then give w_n and ρ_n in terms of p_n.

The barotropic mode is not included in the sums of (10) because for the steady solutions found in this paper the barotropic mode is exactly in Sverdrup balance (see the discussion of equations (34)). For winds with no curl this state consists of a weak barotropic pressure gradient force (sea level slope) that balances the wind, and there is no contribution to the flow field. The sum over the infinite number of baroclinic modes is necessarily truncated at a finite value, N. So, this method of solution will be of value only if the series converge rapidly enough with n so that N need not be too large. As we shall see for realistic choices of $\rho_\mathrm{b}(z)$ and ν, rapid convergence is assured.

Note that the effects of vertical friction enter equations (11) as simple linear drag with drag coefficients, ω_n or ω_n/σ, as in the Yoshida (1967) model. However, in the present formalism the values of the drag coefficients are not set arbitrarily, but are closely related to the strength of the diffusive mixing. Because the drag coefficients depend on ϵ_n, their magnitude varies rapidly with n: as $n \to \infty$, $\omega_n \to$ const. $\times n^2$. As we shall see, this dependency of drag on mode number is a very important aspect of the model dynamics.

It is possible to include a constant-thickness, surface mixed layer in the model simply by assuming that $N_\mathrm{b}(z) = 0$ for $z > -H$. The eigenfunction problem as defined in (6)–(8) is still well posed, and so the eigenfunctions as well as the solutions (10) remain well behaved. An important effect of the mixed layer is that $\psi_{nz} = 0$ there. As a result, in the mixed layer u, v and p are independent of z, w varies linearly with z, and ρ is identically zero. Other properties and limitations of this mixed layer formulation are discussed in greater detail in McCreary (1981).

The relation of the present model to those studied by several previous workers is now evident. The equations of motion of Lighthill (1969) and of Gill & Clarke (1974) can be recovered from (11) by setting $\omega_n = \nu_\mathrm{h} = \kappa_\mathrm{h} = 0$. The equations of motion of Yoshida (1967) are essentially equations (11) with $\partial_t = \nu_\mathrm{h} = \kappa_\mathrm{h} = 0$; however, Yoshida obtained solutions only for a single baroclinic mode.

3. The solution

In this section solutions to (11) are found for a steady wind field of the form

$$\tau^y = \tau_0 Y(y), \quad \tau^x = 0, \tag{14}$$

so that

$$G_n = \tau_0 Y(y) \Big/ \int_{-D}^{0} \psi_n^2 \, \mathrm{d}z \equiv \tau_{0n} Y(y), \quad F_n = 0, \tag{15}$$

where τ_{0n} is obviously defined. $Y(y)$ is an arbitrary function of y, which is non-zero in a region of finite extent, and which does not extend to the equator. The wind field is independent of x, and therefore has no curl. So, the model is forced by a mid-latitude band of meridional winds (as in figure 3). It is an easy extension of the procedure described below to include the effects of both zonal winds and wind curl. Both are ignored here because neither property is essential for the existence of the Coastal Undercurrent.

The eastern boundary of the model ocean consists of a vertical barrier at $x = 0$. Since there can be no flow through this barrier, solutions to (11) must satisfy the boundary condition

$$u_n = 0 \quad \text{at} \quad x = 0. \tag{16a}$$

The ocean is unbounded to the west, north and south. Solutions must therefore satisfy the additional constraint that

there are no sources of energy (other than the wind) at $x = -\infty$ or $y = \pm\infty$. (16*b*)

This condition means that solutions must remain finite in the far field.

Even though the driving wind field is steady and has a simple spatial structure, solutions to (11) are still difficult to find. Two additional restrictions greatly reduce the required level of algebra. First, the horizontal mixing of heat and momentum is neglected by setting $\nu_h = \kappa_h = 0$. The inclusion of these processes in the model, and their effect on the coastal currents, is dealt with separately in the Appendix. Second, the alongshore velocity field is assumed to be in geostrophic balance. This approximation is common to virtually all models of coastal circulation and is very accurate, provided that the alongshore scale of the wind field is much larger than the Rossby radius of deformation of the $n = 1$ baroclinic mode (roughly 30 km at mid-latitudes). In addition, the observed variability in the strength of coastal jets is consistent with alongshore geostrophy (Allen 1980).

Many of the quantities involved in the remainder of this paper depend in some way on the eigenvalue, c_n. For that reason they should be labelled with a subscript, n. For notational simplicity this subscript is subsequently deleted from the following quantities: c, ω, α, k, l, Λ, P, G.

Consistent with the specified wind field and the above restrictions, the first three equations of (11) can be rewritten

$$\left.\begin{aligned} v_n &= \frac{p_{nx}}{f}, \\ u_n &= \frac{G}{f} - \frac{p_{ny}}{f} - \frac{\omega}{f^2} p_{nx}, \\ p_{nxx} + \frac{\beta}{\omega} p_{nx} - \frac{\alpha^2}{\sigma} p_n &= 0. \end{aligned}\right\} \tag{17}$$

where β is the meridional derivative of f, and $\alpha^{-1} = c/f$ is the Rossby radius of deformation of the nth baroclinic mode.

In an unbounded ocean the solution to (17) is trivial. Since the wind stress is independent of x, so is the solution. The unbounded solution, designated by a prime, is therefore

$$u_n' = G/f, \quad v_n' = 0, \quad p_n' = 0. \tag{18}$$

None of the fields of (18) involves the eigenvalue c, and consequently the sums (10) can be calculated explicitly. It follows that in the surface mixed layer there is a uniform drift of amplitude $[(D-H)/DH]\tau^y/f$, and below the mixed layer there is a compensating return flow at the velocity $-\tau^y/Df$. It is useful to refer to this solution as the Ekman flow associated with the model ocean.

When there is an eastern boundary, (18) is only one component of the complete flow field. The boundary is a source of another component. Since (18) is already in balance with the wind field, the boundary component must be a solution of (17) with $G \equiv 0$. The boundary solution, designated by a double prime, can be written

$$p_n'' = P(y)\, e^{k(y)\,x}, \tag{19a}$$

so that

$$\left.\begin{aligned} v_n'' &= \frac{k}{f} P \mathrm{e}^{kx}, \\ u_n'' &= -\frac{1}{f}\left(\partial_y + \frac{\omega k}{f}\right) P \mathrm{e}^{kx}, \end{aligned}\right\} \tag{19b}$$

where $P(y)$ is, as yet, an unspecified function of y. The function, $k(y)$, is fixed by the third equation of (17) to be one of the two roots of the quadratic

$$k^2 + \frac{\beta}{\omega} k - \frac{\alpha^2}{\sigma} = 0, \tag{20}$$

and to satisfy the boundary condition (16b) k must be the root

$$k = -\frac{\beta}{2\omega}\left[1 - \left(1 - 4\frac{\omega^2}{\beta^2}\frac{\alpha^2}{\sigma}\right)^{\frac{1}{2}}\right]. \tag{21}$$

The advantage of the assumption of alongshore geostrophy is now clear. Without the use of that assumption the third equation of (17) involves the term, p_{nyy}, and so it is not possible to look for solutions in the separable form (19a).

The boundary condition (16a) requires that u_n' and u_n'' sum to zero at $x = 0$. Therefore, $P(y)$ must satisfy the differential equation

$$(\partial_y + \omega k/f)\, P = G. \tag{22}$$

The solution to (22) is

$$P = \mathrm{e}^{-\Lambda} \int_{y_0}^{y} \mathrm{e}^{\Lambda} G \,\mathrm{d}y, \tag{23}$$

where y_0 is any position that lies equatorward of the wind band, and

$$\Lambda = \int^{y} \frac{\omega k}{f} \mathrm{d}y. \tag{24}$$

The choice of lower limit in (23) ensures that the condition (16b) is satisfied; any other choice allows an exponentially growing solution in the far field. The choice of lower limit in (24) is arbitrary. With P known, so are the solutions u_n'', v_n'' and p_n''.

The desired solution is the sum of primed and double-primed fields, that is

$$\left.\begin{aligned} p_n &= \left\{\tau_{0n} \int_{y_0}^{y} \mathrm{e}^{\Lambda}\, Y(y)\, \mathrm{d}y\right\} \mathrm{e}^{kx}\, \mathrm{e}^{-\Lambda}, \\ v_n &= \frac{k}{f} p_n, \\ u_n &= \tau_{0n} \frac{Y}{f}(1 - \mathrm{e}^{kx}) - \frac{x}{f} k_y p_n. \end{aligned}\right\} \tag{25}$$

The complete three-dimensional flow field is then determined by the use of (25) in (10). The integral in (25) and the summations in (10) cannot be evaluated analytically, but they are easy to determine numerically with the aid of a computer.

Important properties of the solution are evident from the structure of the p_n-field. Note that the amplitude of p_n (the expression in curly brackets) is proportional to an integral of Y, rather than to Y itself. Therefore p_n does not vanish poleward of the wind band. Instead, p_n is proportional to $\mathrm{e}^{-\Lambda}$ there, and so decays poleward with an alongshore decay scale, l^{-1}, where

$$l \equiv -\mathrm{e}^{\Lambda}(\mathrm{e}^{-\Lambda})_y = \Lambda_y = \omega k/f. \tag{26}$$

PHILOSOPHICAL TRANSACTIONS OF THE ROYAL SOCIETY A MATHEMATICAL, PHYSICAL & ENGINEERING SCIENCES

The offshore decay scale of p_n is k^{-1}. Both l and k are monotonically increasing functions of the drag coefficient, ω. As a result, as ω increases the solution becomes more coastally trapped and more latitudinally confined to the region of the wind band. As we shall see in § 5, this change in horizontal structure reflects a change in the underlying dynamics as well.

4. Results

The model was used to study the response of the ocean to a wind field of the form (14) with $\tau_0 = -0.5\,\mathrm{dyn/cm^2}$, and

$$Y(y) = \begin{cases} (y-y_0)/\Delta y, & y_0 \leqslant y < y_0+\Delta y, \\ 1, & y_0+\Delta y \leqslant y < y_0+3\Delta y, \\ -(y-y_0-4\Delta y)/\Delta y, & y_0+3\Delta y \leqslant y < y_0+4\Delta y, \\ 0, & \text{otherwise}, \end{cases} \tag{27}$$

where $\Delta y = 10° \times (\pi/180°) \times R$, $y_0 = 20° \times (\pi/180°) \times R$, and R is the radius of the Earth. This wind field was chosen to resemble the steady component of the winds off the western coast of North America (Nelson 1976). The shaded region of figure 3 indicates the location of the wind band, and the thin line its meridional profile, (27).

There is no restriction on f or β in this ocean model. Unless stated otherwise,

$$f = 2\Omega \sin y/R, \quad \beta = (2\Omega/R)\cos y/R, \tag{28}$$

where $\Omega = 2\pi\ \mathrm{day}^{-1}$.

Figure 2 shows seven different profiles of background density structure, $\rho_\mathrm{b}(z)$. Profile 1 varies linearly beneath a surface mixed layer of thickness $H = 50\,\mathrm{m}$. The remaining curves are described by

$$\rho_\mathrm{b}(z) = \begin{cases} 1, & z \geqslant -H, \\ 1+\Delta\rho_1[1-\mathrm{e}^{-(z+H)/b_1}] & \\ \quad +\Delta\rho_2[1-\mathrm{e}^{-(z+H)/b_2}], & -D \leqslant z < -H, \end{cases} \tag{29}$$

where $b_1 = 200\,\mathrm{m}$, $b_2 = 1000\,\mathrm{m}$, and the depth of the ocean is $D = 2500\,\mathrm{m}$. For profile 2, $\Delta\rho_1 = 0$, $\Delta\rho_2 = 0.0035$, and $H = 50\,\mathrm{m}$. For profile 3, $\Delta\rho_1 = 0.00225$, $\Delta\rho_2 = 0.00125$, and $H = 50\,\mathrm{m}$. The unlabelled curves all have $\Delta\rho_1 = 0.00125$, $\Delta\rho_2 = 0.00225$. They differ only in that $H = 0\,\mathrm{m}$, 25 m, 50 m and 75 m. Unless stated otherwise, $\rho_\mathrm{b}(z)$ is always given by the thicker curve. This profile is typical of the density structure off the coast of California.

For all results the Prandtl number is unity, that is $\sigma = 1$. The mixing coefficients, $\nu = \kappa = A/N_\mathrm{b}^2$, vary considerably with depth. Just beneath the mixed layer, where N_b^2 attains its maximum value, ν reaches a minimum, ν_min. At greater depths ν increases monotonically. Unless stated otherwise, A is set so that $\nu_\mathrm{min} = 10\,\mathrm{cm^2/s}$. When $\rho_\mathrm{b}(z)$ is the thicker curve of figure 3, the value of ν at 200 m (approximately the core of the Coastal Undercurrent) is $17\,\mathrm{cm^2/s}$, and at the ocean bottom ν is an unrealistically large $438\,\mathrm{cm^2/s}$. The large bottom value, however, does not significantly affect the structure of the solution (see the discussion of figure 6).

It is necessary to choose a sufficiently large value of N in the sums (10). In a series of tests N was varied over a wide range of values, and solutions were compared. For $N \geqslant 50$ they were virtually identical. The solutions discussed here have $N = 100$, and so they are adequately resolved.

PHILOSOPHICAL TRANSACTIONS OF THE ROYAL SOCIETY A MATHEMATICAL, PHYSICAL & ENGINEERING SCIENCES

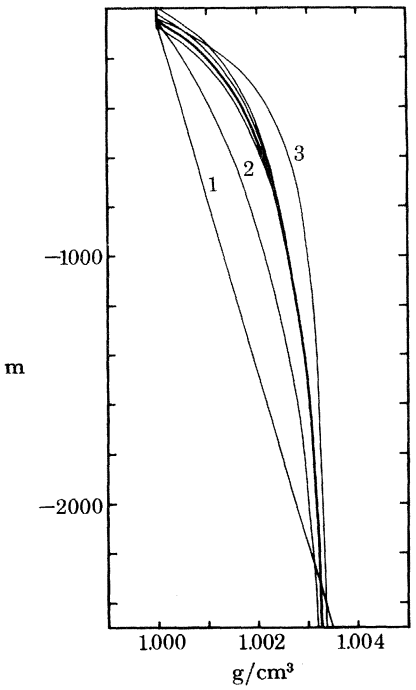

FIGURE 2. Profiles of background density structure, $\rho_b(z)$. Profile 1 has a constant gradient below the mixed layer. The remaining profiles are described by equation (29). The unlabelled curves differ only in the thickness of the surface mixed layer. Most results correspond to the thicker curve.

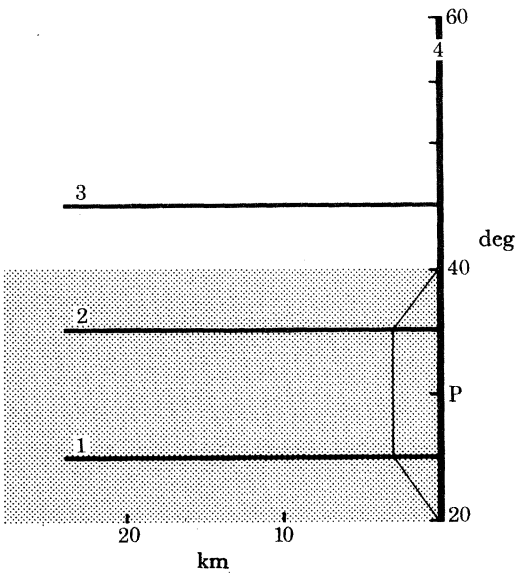

FIGURE 3. A schematic diagram showing the locations of sections 1–4, the position of the coast, and the structure of the wind band. The shaded region indicates the latitudinal extent of the wind field, and the thin line its meridional profile. The wind field does not weaken offshore, and so it is without curl. Wind stress is entirely equatorward and reaches a maximum amplitude of 0.5 dyn/cm². The structure of the wind field is described more precisely in equation (27).

(*a*) *The model Undercurrent*

Four sections describe the three-dimensional flow field. Figure 3 shows their positions relative to the driving wind. Figures 4*a–d* show the alongshore and transverse circulation patterns of sections 1–4, respectively. Figures 4*a–c* also indicate the structure of the density field.

The alongshore flow field has features that compare favourably with those observed. There is a poleward current situated in the main thermocline beneath the surface mixed layer. Its speed increases to a maximum of 36 cm/sec near the northern edge of the wind band at 35° N. Both the thickness and the depth of the current increase to the north. For example, at 30° N the current extends from 100 to 300 m with its core at 150 m, whereas at 50° N poleward flow exists from 150 m to nearly 500 m with a maximum at 250 m. Surface equatorward flow reaches a maximum of 64 cm/s, again at 35° N. The e-folding width scale of both currents is roughly 6 km. The coastal currents extend well north of 40° N, so that they are entirely remotely driven there by the winds to the south.

The transverse flow field also agrees well with observed upwelling circulation patterns. In the region of the wind band there is offshore surface drift of the order of 1 cm/s. As a result, there is a divergence of fluid from the coast, and upwelling into the surface layer occurs at speeds as large as 0.015 cm/s. The upwelling does not occur throughout the water column, but is confined above the core of the Undercurrent. At greater depths there is weak downwelling. The strongest onshore flow occurs at and slightly above the current core at speeds somewhat less than 1 cm/s. In contrast to the alongshore flow, strong transverse circulation is confined to the region of the wind band, and so is predominantly locally forced by the wind. The sign and amplitude of v_y determine the strength of convergence or divergence of fluid from the core. The weak transverse circulation pattern along section 3, where there is no wind, is driven entirely by this effect.

The density field, that is $\rho_b(z) + \rho(x, y, z)$, also has expected features. Consistent with alongshore geostrophy, isopycnals at depths less than that of the Undercurrent core bend upward, and isopycnals at greater depths bend downward. This spreading of isopycnals is greatest along section 2 where the speed of the Undercurrent is largest.

Coastal sea level decreases from 20° to 38° N by 8 cm, and then gradually increases farther poleward. There is a maximum poleward sea level inclination at 26° N somewhat less than -5×10^{-8}, equivalent to a surface pressure gradient force of 5×10^{-5} dyn/g. The maximum equatorward surface pressure gradient force of 1.6×10^{-5} dyn/g occurs just poleward of the wind band at 41° N. At the depth of the core of the Undercurrent the pressure gradient force is everywhere poleward, but much weaker than the surface maximum. Slightly below the current core (50–100 m deeper) the pressure gradient force vanishes and at greater depths becomes weakly equatorward. This pressure field is consistent with the observations off the coast of California discussed in the Introduction.

(*b*) *The dependence on model parameters*

It is important to know how the response of the model varies with the choice of free parameters. Since $\nu_h = \kappa_h = 0$ and $\sigma = 1$ there are only two: $\rho_b(z)$ and ν. Do solutions vary significantly as the value of the amplitude of mixing near the core of the Undercurrent changes? Does the response depend critically on the vertical structure of ν? Is the presence of a near-surface pycnocline or the existence of a surface mixed layer necessary for the generation of a realistic Undercurrent? To answer such questions figures 5, 6 and 7 compare profiles of alongshore

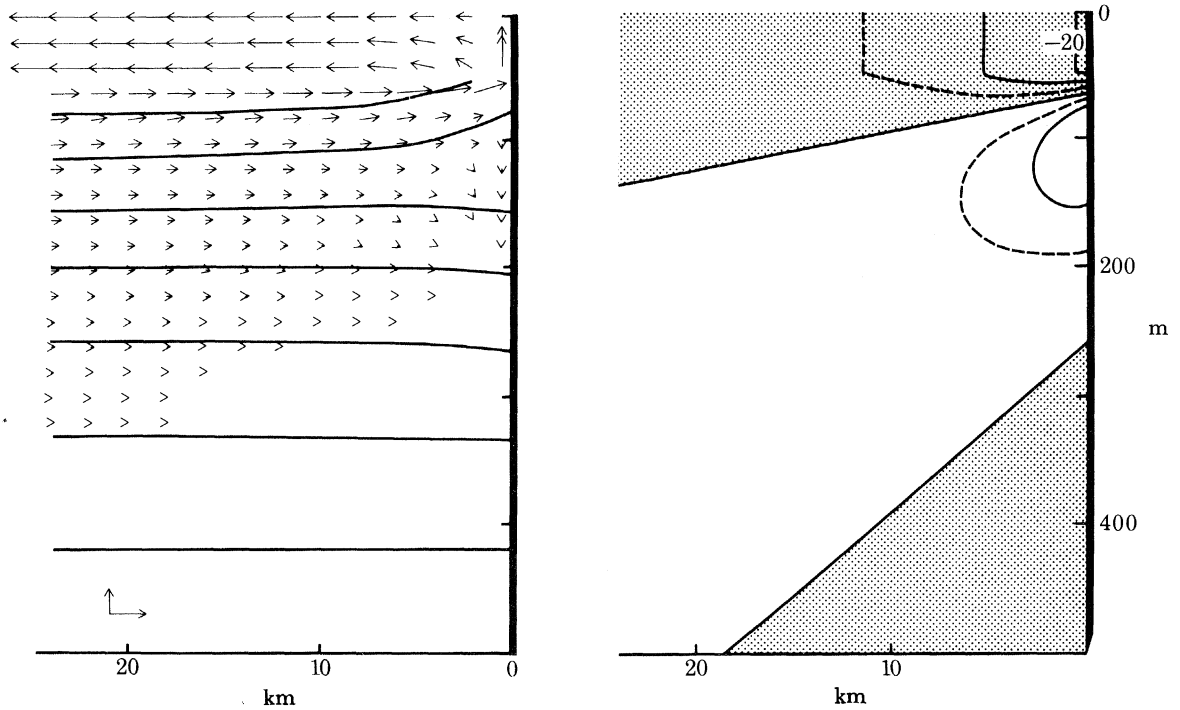

FIGURE 4*a*. Vertical sections of transverse circulation and density structure (left panel), as well as alongshore current (right panel) along section 1 of figure 3. The velocity contour interval is 10 cm/s; the dashed contours are ± 5 cm/s. Calibration vectors in the lower left corner of the left panel have amplitudes of 0.01 cm/s and 1 cm/s in the vertical and horizontal directions, respectively. The density of the surface mixed layer is uniformly 1 g/cm³; the isopycnal contour interval is 0.00025 g/cm³, and the uppermost isopycnal has the value 1.00025 g/cm³.

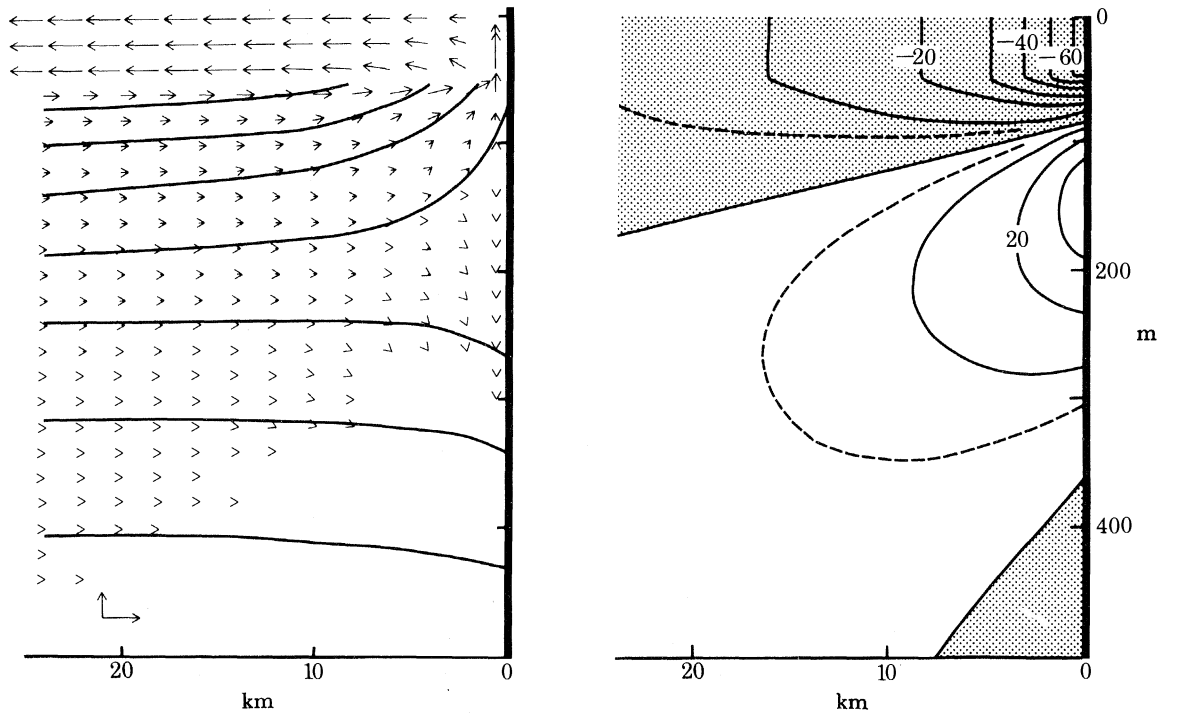

FIGURE 4*b*. As for figure 4*a*, but along section 2.

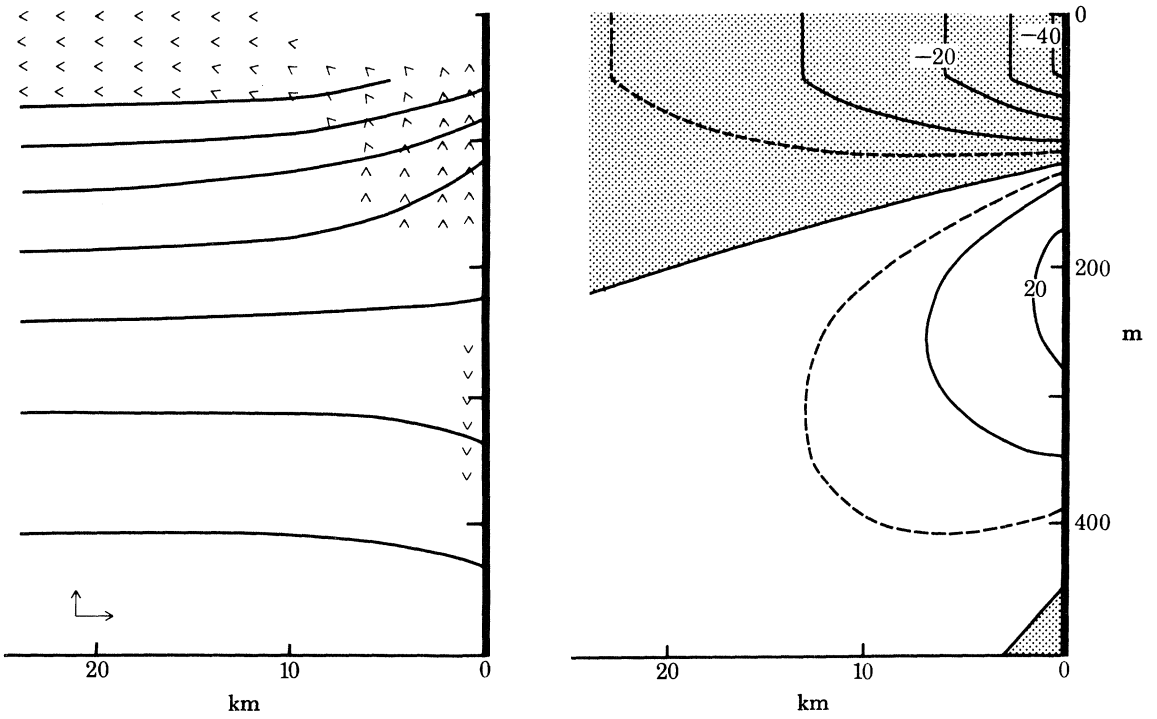

FIGURE 4*c*. As for figure 4*a*, but along section 3.

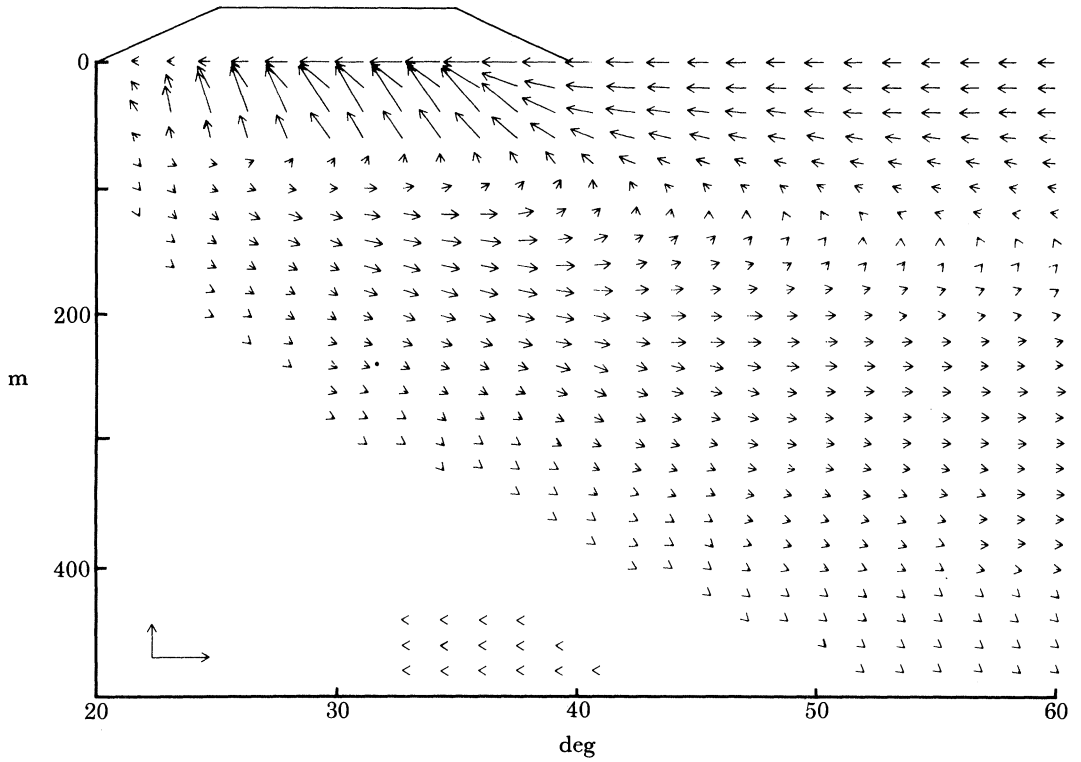

FIGURE 4*d*. Velocity section along section 4 of figure 3. Calibration vectors in the lower left corner of the figure are 0.01 cm/s and 100 cm/s in the vertical and horizontal directions, respectively. The thin line indicates the meridional profile of the wind field. The alongshore current extends well poleward of the region of the wind band, but the upwelling does not.

PHILOSOPHICAL TRANSACTIONS OF THE ROYAL SOCIETY A MATHEMATICAL, PHYSICAL & ENGINEERING SCIENCES

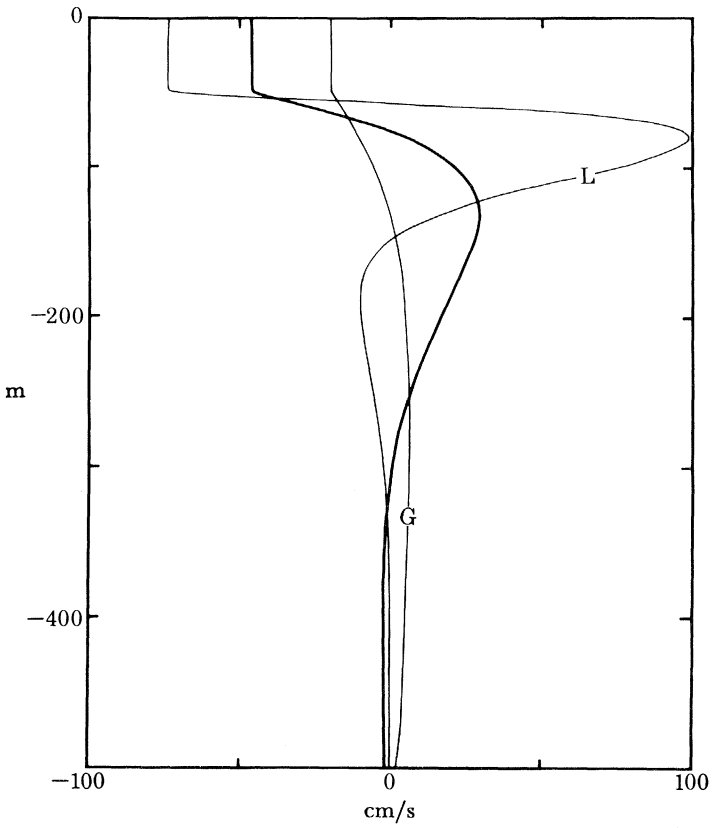

FIGURE 5. Profiles of alongshore current (cm/s) at point P of figure 3 contrasting the model response for three different values of ν_{min}. Profiles G and L correspond to $\nu_{min} = 100$ and 1 cm²/s, respectively. The structure of the flow varies more weakly than $\nu_{min}^{\pm 1}$.

currents over a wide range of parameter values. All profiles are taken at the centre of the wind band, that is, point P of figure 3. In each figure the thicker reference curve is just that of the model Undercurrent discussed previously.

Figure 5 compares solutions in which ν_{min} varies but $\rho_b(z)$ remains fixed (only the parameter A of (2) is changed). In this way the amplitude of ν changes, but not its structure with depth. Profiles G and L show the model response when $\nu_{min} = 100$ and 1 cm²/s, respectively. As ν_{min} weakens, the Undercurrent becomes stronger and shallower. Although the structure of the solutions does depend on ν_{min}, that dependence is weaker than might be expected. For example, while ν_{min} decreases by two orders of magnitude, the maximum speed of the Undercurrent increases only by a factor of 17, and the depth of the current core shallows by a factor of 4. Similarly, the e-folding width scale of the jet (not shown in the figure) decreases by a factor of 4. All of these measures of the flow field vary more weakly with the mixing parameter than ν_{min}^{+1} or ν_{min}^{-1}.

Figure 6 compares solutions in which the deep density structure of the ocean varies but ν_{min} remains fixed at 1 cm²/s. In this way the vertical structure of ν changes but its amplitude in the vicinity of the Undercurrent does not. Profiles 1, 2 and 3 show the model response for curves 1, 2 and 3 of figure 2, respectively. As the pycnocline becomes increasingly confined to the surface the Undercurrent becomes weaker and shallower. There is no indication that its width changes. Clearly the model is very insensitive to changes in the deeper density structure of the ocean. It

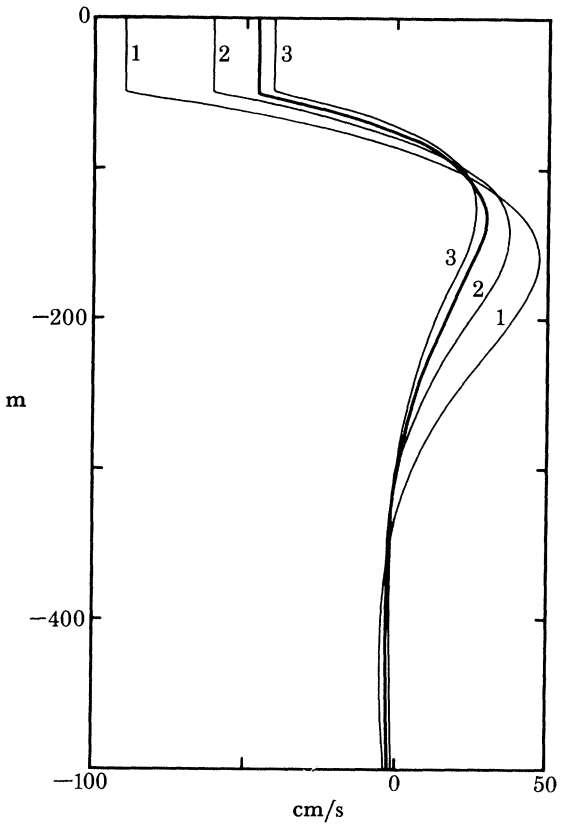

FIGURE 6. Profiles of alongshore current (cm/s) at point P of figure 3 contrasting the model response for four different background density structures. Profiles 1, 2 and 3 correspond to curves 1, 2 and 3 of figure 2, respectively. The thicker profile corresponds to the thicker curve of figure 2. The profiles are very insensitive to the shape of $\rho_b(z)$ beneath the mixed layer.

also follows that the model is quite independent of the size of mixing coefficients in the deep ocean, even though they can be very large there.

Figure 7 compares solutions in which only the depth of the mixed layer is changed; the shape of the pycnocline is unaltered, and the value of $\nu_{\min}$ remains fixed at 1 cm²/s. The profiles show the model response for the unlabelled curves of figure 2. As H decreases the Undercurrent becomes moderately stronger and shallower. Again, there is no appreciable change in its width. The strength of the surface equatorward drift, however, changes markedly. When $H = 0$ this flow attains the large value of -160 cm/s; in addition, the surface Ekman flow becomes infinitely large (see the discussion of equations (18)). Clearly, the presence of a sufficiently thick ($25 \lesssim H \lesssim 50$ m) turbulent surface mixed layer is necessary in this model to obtain realistic surface flows. The structure of the deeper currents is not strongly affected by changes in H.

(c) *The f-plane response*

How important is the β-effect for the generation of the model Coastal Undercurrent? To provide some insight into this question it is useful to find the response of the present model on the f-plane. The f-plane response can be found simply by taking the limit $\beta \to 0$ in (25). In that case,

$$k = \sigma^{-\frac{1}{2}}\alpha, \quad p_n = \left\{\tau_{0n}\int_{y_0}^{y} e^{(\omega/c)y}\, Y\, dy\right\} e^{-(\omega/c)y}\, e^{kx}, \tag{30}$$

and the other fields of (25) are modified accordingly.

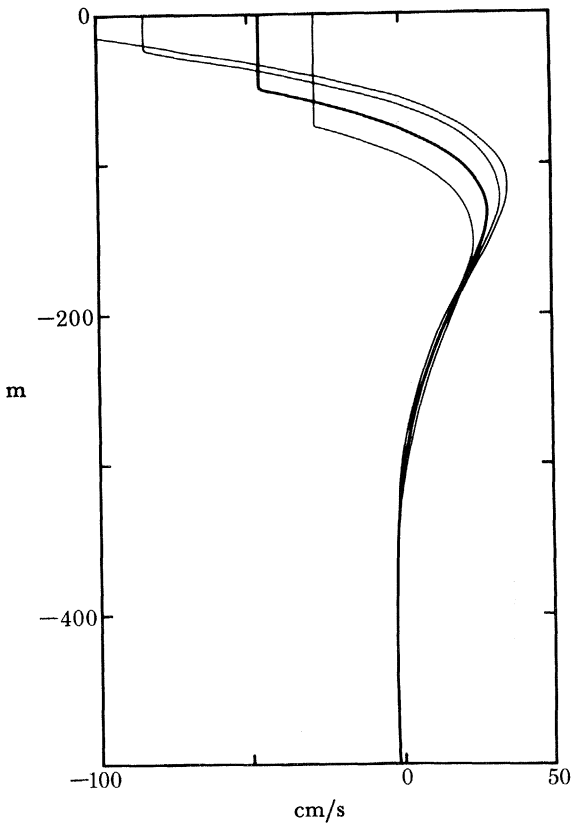

FIGURE 7. Profiles of alongshore current (cm/s) at point P of figure 3 contrasting the model response for four different values of mixed layer depth, H. The profiles correspond to the four unlabelled curves of figure 2. When $H = 0$ the surface velocity is -160 cm/s. The surface mixed layer is necessary to obtain realistic surface velocities, but other aspects of the flow depend weakly on H.

Figure 8 shows a transverse section of the f-plane flow field that is comparable with figure 4b; the driving winds and model parameters are the same, and both sections are along section 2 of figure 3. The two figures are very similar. Without β, the Undercurrent is somewhat deeper and weaker, and the equatorward surface drift is stronger. The transverse circulation patterns are virtually identical. Evidently, the β-effect is not necessary to generate a realistic Coastal Undercurrent.

However, this conclusion is valid only for the x-independent wind field of interest here. Suppose that at some distance offshore τ^y gradually decreases to zero, so that in the interior ocean there is a region of non-zero wind curl. Then in that region the f-plane model described above spins up to unrealistically large levels. The reason for this is that a bottom Ekman layer, not allowed by the boundary conditions (4), is now necessary. Consider the following argument. Beneath the surface Ekman layer the interior flow field is geostrophically balanced, and so

$$w_z = -(u_x + v_y) = (\beta/f)\, v. \tag{31}$$

When $\beta \neq 0$, w can be depth-dependent, and it weakens with depth. When $\beta = 0$, w is necessarily depth-independent. A bottom Ekman layer is then required to absorb the flow downwelling from the ocean surface. The onshore transport of the lower Ekman layer extends back to the coast and modifies the flow field of figure 8 considerably (Allen 1973; Pedlosky 1974).

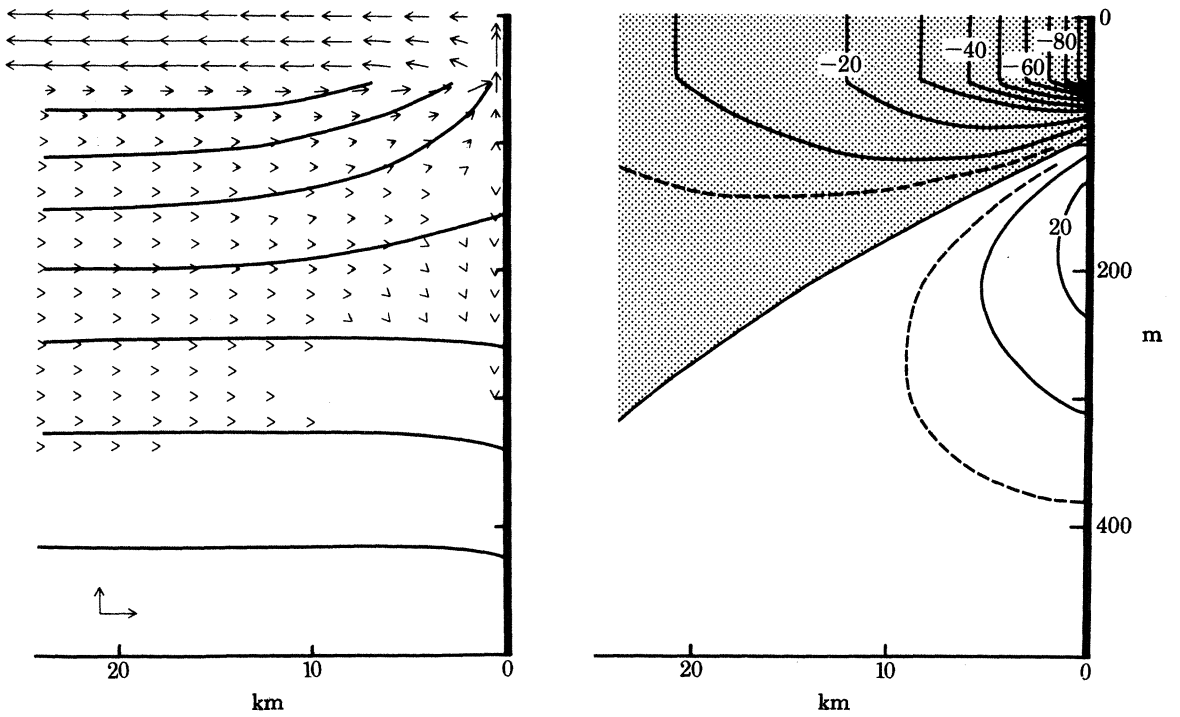

FIGURE 8. Vertical sections of f-plane flow, described by equations (30), showing transverse circulation and isopycnal structure (left panel) as well as alongshore current (right panel) along section 2 of figure 3. Contour intervals and calibration vectors are the same as in figure 4a. The surface equatorward drift is intensified, and the Coastal Undercurrent is weakened.

5. DYNAMICS

The method of solution adopted here, that is the expansion into vertical normal modes, allows a very useful way of discussing the dynamics of the model. Rather than describing the dominant balances governing the total flow field, it is possible to describe those balances that occur for individual modes. In this way the three-dimensional dynamics of equations (1) can be understood with the use of concepts appropriate to the two-dimensional dynamics of equations (11).

An important feature of the model is that low-order modes behave very differently from high-order modes. So, in the first part of this section simpler models are discussed that illustrate these differences. Because the flow fields generated by these simpler models have very unrealistic features, they also serve to demonstrate that both the alongshore baroclinic pressure gradient field and vertical mixing are essential elements in the dynamics of the Coastal Undercurrent.

(a) *Simpler models*

A model that illustrates the importance of the establishment of the alongshore baroclinic pressure gradient field in coastal circulation ignores the terms p_{ny} and v_{ny} in equations (11). In that

$$k = \sigma^{-\frac{1}{2}}\alpha, \quad p_n = (f/\omega k)\,\tau_{0n}\,Y(y)\,e^{kx}, \tag{32}$$

case, and the other fields of (25) are modified accordingly. Note that the solution is directly proportional to Y, and therefore does not extend poleward of the wind band. It is useful to refer to a single baroclinic mode described by (32) as being in a two-dimensional or local balance, and to a coastal flow field in which all baroclinic modes have this form as a two-dimensional flow.

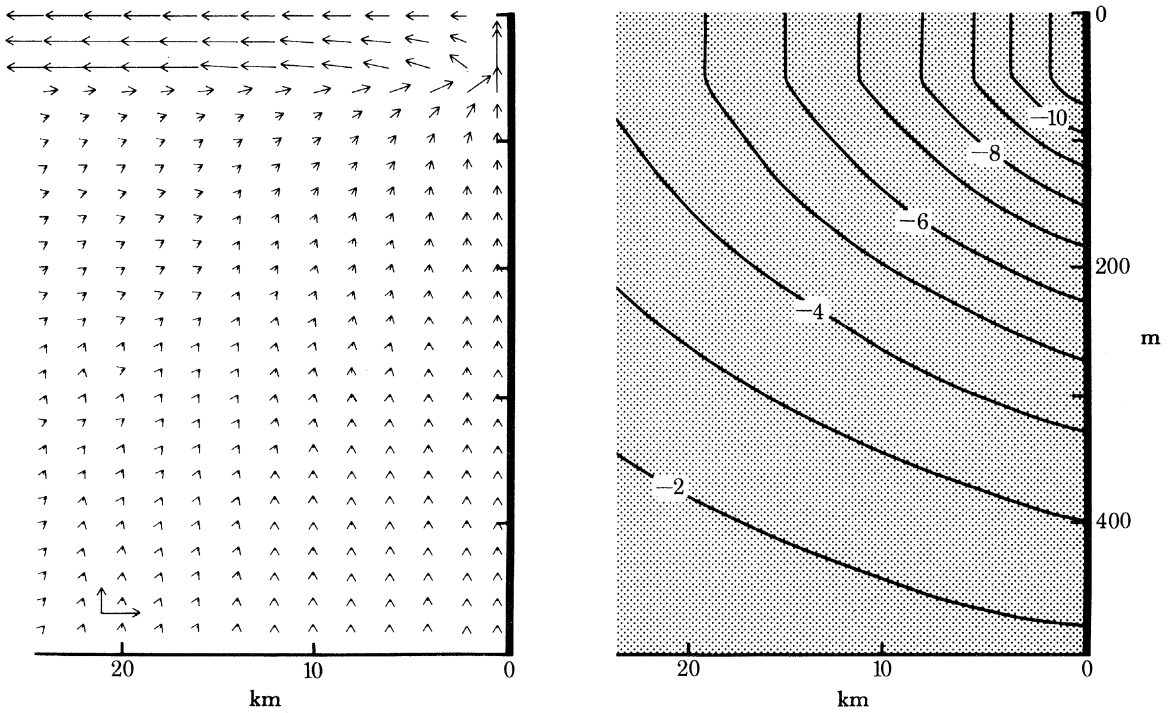

FIGURE 9. Vertical sections of two-dimensional flow, described by equations (32), showing transverse circulation (left panel) and alongshore current (right panel) along section 2 of figure 3. The contour interval is 1 km/s. Calibration vectors in the lower left corner of the left panel have amplitudes 0.01 cm/s and 1 cm/s in the vertical and horizontal directions, respectively. The unrealistic alongshore flow field demonstrates the importance of the establishment of the alongshore baroclinic pressure field gradient in the coastal ocean.

Figure 9 shows a transverse section of a two-dimensional flow field that is otherwise comparable with figure 4*b*. The transverse circulation pattern of figure 9 is quite reasonable. It closely resembles that of figure 4*b* in both magnitude and structure. The major difference is that in figure 9 coastal upwelling is not confined to the upper 100 m, but rather extends to the ocean bottom. However, the alongshore currents are ludicrously large and not at all surface-trapped. Poleward flow exists only at depths greater than 700 m. Apparently, alongshore baroclinic pressure gradients, p_{ny}, are essential for limiting alongshore currents and for keeping the flow field confined near the ocean surface.

The mathematical reasons for the limitations of the two-dimensional model are evident in the form of (32). It follows that at the coast $v_n = (c^2/A)\,G$. Since G decreases with n, and c^2 varies very much like n^{-2}, v_n drops off rapidly with increasing mode number. So the two-dimensional model strongly favours the low-order modes. The vertical structure of the alongshore current must look very much like the first baroclinic mode, and so there can be no surface trapping. There is no mechanism in the two-dimensional model that can inhibit the strength of the low-order modes.

A model that illustrates the importance of vertical mixing in the coastal ocean ignores the drag terms in (11). The response of the inviscid model can be found from (25) by setting $\sigma = 1$ and then taking the limit $\omega \to 0$. On the f-plane, the solution (25) is simplified by the replacements

$$k = \alpha, \quad p_n = \tau_{0n} \int_{y_0}^{y} Y \,\mathrm{d}y \,\mathrm{e}^{kx}. \tag{33}$$

On the β-plane,

$$k = 0, \quad p_n = \tau_{0n} \int_{y_0}^{y} Y \,\mathrm{d}y. \tag{34}$$

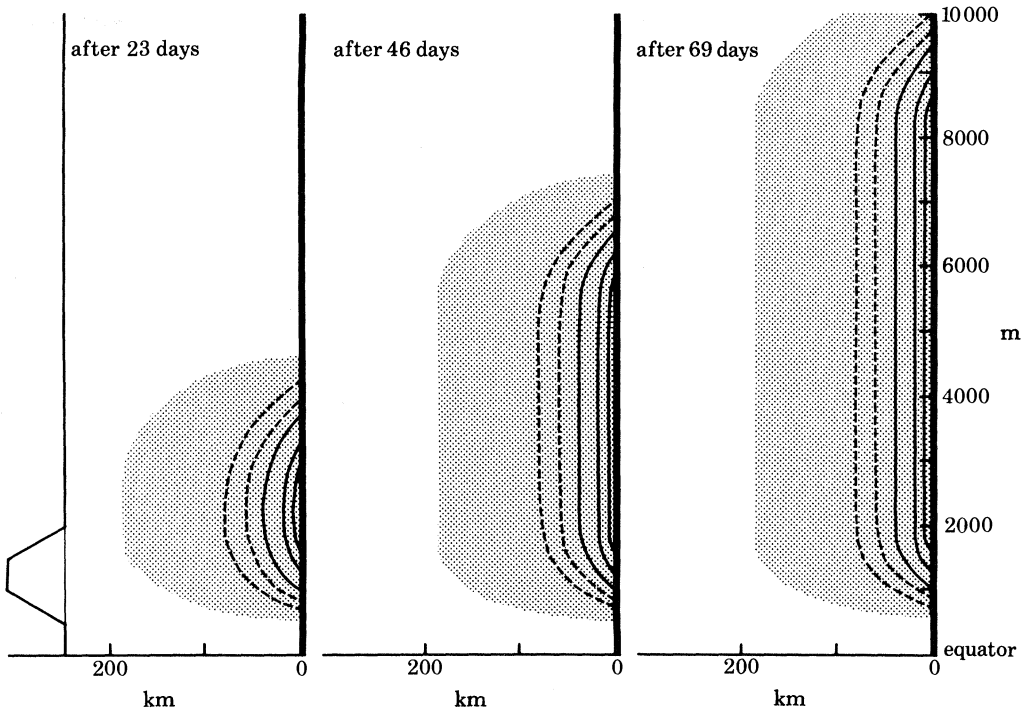

FIGURE 10. The adjustment of a baroclinic mode to the f-plane inviscid balance, (33). The figure shows contours of surface alongshore current, v, and also of sea level, d. The velocity contour interval is -10 cm/s; dashed contours are -5 and -2.5 cm/s. At the coast the equatorward current is -35 cm/s. The shaded region indicates equatorward flow less than -0.5 cm/s. Sea level contours (cm) are related to velocity contours by the expression $d = (c/g)\, v$. The thin line in the left panel represents the meridional profile of the driving wind band. Parameters are $c = 141$ cm/s and $f = 5 \times 10^{-5}$ s^{-1}; the minimum value of G is -5×10^{-5} cm/s^2. The rapid poleward propagation of a Kelvin wave sets up a coastal jet. After McCreary (1977, 1978).

It is useful to refer to a baroclinic mode described by (33) or (34) as being in an inviscid balance and to an oceanic flow in which all the modes have one or other of these forms as an inviscid ocean flow. Equations (34) are a special case of the solution obtained by Sverdrup (1947) in describing the depth-averaged properties of oceanic flow. It is therefore also sensible to refer to a baroclinic mode described by (34) as being in Sverdrup balance, and a flow field with all modes described by (34) as a baroclinic Sverdrup flow.

The responses described in (33) and (34) are interesting in that they extend poleward of the region of the wind band, and when $\beta \neq 0$ they extend offshore as well. The radiation of Kelvin and Rossby waves is crucial for the adjustment of baroclinic modes to these highly non-local steady states. Suppose that a wind band, similar to that of figure 3, is switched on at some initial time. Figure 10, adapted from McCreary (1977, 1978), traces the adjustment on the f-plane. Immediately there is offshore Ekman drift in the region of the wind band. An upwelling signal propagates rapidly poleward in the form of a coastal Kelvin wave. In the wake of the Kelvin wave front the inviscid balance (33) is set up. Associated with this balance is a coastal jet, and this current provides the source of water for the Ekman drift. Figure 11, adapted from McCreary (1976), traces the adjustment when $\beta \neq 0$. As in figure 10, the radiation of Kelvin waves initially generates a coastal jet. However, the jet does not remain trapped to the coast; instead, it propagates offshore as a Rossby wave. Behind the Rossby wave front the mode is adjusted to the Sverdrup balance (34).

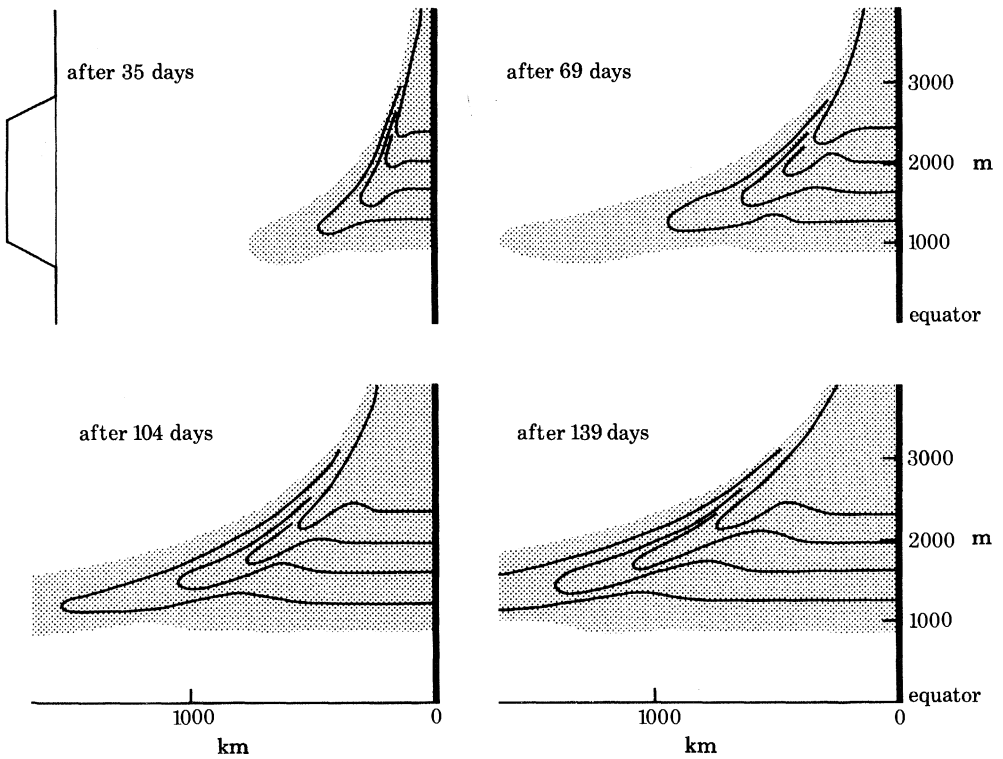

FIGURE 11. The adjustment of a baroclinic mode to Sverdrup balance, (34). The figure shows contours of sea level. The contour interval is -1 cm, and the shaded region indicates a change in sea level of less than -0.2 cm. The thin line in the upper left panel represents the meridional profile of the driving wind band. The value of c is 282 cm/s, and the minimum value of G is -2.5×10^{-5} cm/s^2. The existence of Rossby waves allows the coastal jet of figure 10 to propagate offshore. After McCreary (1976).

Inviscid flows do not have a realistic coastal current structure. When $\beta \neq 0$ the sum over all modes can be made explicitly, since none of the fields involves c. The solution has no currents anywhere in the ocean; instead, an alongshore pressure gradient exists in the surface mixed layer which everywhere balances the wind. On the f-plane, the same mixed layer pressure gradient exists at the coast, but decays rapidly offshore. The geostrophic alongshore currents in balance with this pressure field are not well defined in the upwelling corner. For example, the Coastal Undercurrent in this model has the character of a Dirac δ-function; that is, it appears as an infinitesimally narrow, infinitely strong jet at the base of the mixed layer. (This singular flow field is very much like those that occur in the models of Pedlosky (1969) and Barcilon (1971); see the discussion in the Appendix.) Clearly the vertical mixing of heat and momentum cannot be neglected in the coastal ocean.

(*b*) *The present model*

Recall that the size of the drag coefficient, ω, increases rapidly with mode number, n. As a result both the horizontal structure of the solution, (25), and the underlying dynamics depend on n. Suppose that ω is sufficiently large so that $(\omega/\beta)\,\alpha \gg 1$ and $l\Delta y \gg 1$. Then, to a very good approximation, k and p_n reduce to the form (32). In other words, the high-order modes of the model, where damping is large, tend toward two-dimensional balance. When ω is small enough for $(\omega/\beta)\,\alpha \ll 1$ and $l\Delta y \ll 1$, k and p_n are approximately given by (34). So, a finite number of low-order modes, where damping is weak, can tend toward Sverdrup balance.

The number of modes characterized by Sverdrup balance depends on the magnitude of the mixing parameter, A. In fact, it is possible to choose A so large (unrealistically large) that $l\Delta y \gg 1$ always, and none of the modes approach Sverdrup balance. For the solution of figure 4*b*, A is set (realistically) so that $\nu_{\min} = 10\,\mathrm{cm^2/s}$. For this value of A, $l\Delta y = 1.06$ for $n = 6$, and $l\Delta y = 1.5 \times 10^{-4}$, 0.24, 1.77, and 5.5 for $n = 1$, 4, 7 and 10, respectively. Therefore, modes for $n > 6$ tend to be in two-dimensional balance, and modes for $n < 6$ tend toward Sverdrup balance. The dynamics of the model is neither two-dimensional nor inviscid, but a combination of both. The generation of a realistic coastal current structure requires the presence of modes of both types. The high-order modes in two-dimensional balance reproduce the transverse circulation pattern characteristic of coastal upwelling. The low-order modes tend to adjust to Sverdrup balance by the radiation of Kelvin and Rossby waves, and thereby create alongshore baroclinic pressure gradients that balance the driving wind.

Because the gravest modes can adjust to Sverdrup balance, they do not contribute strongly to the flow field. Instead it is the intermediate modes ($n \approx 6$) that dominate the sums (10). This property is apparent in that the width and depth scales of the currents of figures 4*a–d* have none of the characteristics associated with the gravest modes. For example, the zero crossing of the $n = 1$ mode occurs at a depth greater than 700 m, but the first two zero crossings of the $n = 6$ mode occur at about 85 and 280 m, in good agreement with the solution. The Rossby radius of the $n = 1$ mode at 30° N is 30 km, whereas that of the $n = 6$ mode is 5 km.

Figure 12 illustrates the foregoing ideas. The figure shows the surface velocity contributions of four individual modes to the solution of figures 4*a–d*. The horizontal structures of the currents vary markedly with n. The solution for the $n = 1$ mode is very nearly in Sverdrup balance. The flow field is highly non-local in that it is not at all confined to the region of the wind band, but extends well poleward and offshore. Currents are everywhere weak. The $n = 10$ mode is very nearly in two-dimensional balance. This balance is suggested by the fact that the meridional dependence of the flow field looks very much like $Y(y)$. There is also a divergence of fluid from the coast that is characteristic of offshore Ekman drift there. The intermediate $n = 4$ and $n = 7$ modes are the most strongly excited ones, and they have aspects of both Sverdrup and two-dimensional balances. For the $n = 4$ mode the alongshore decay scale, l^{-1}, is still sufficiently large for the response to extend well poleward of the wind band. However, the offshore decay scale, k^{-1}, is now quite small. As a result, alongshore currents are strong and coastally trapped. The structure of the $n = 7$ mode is similar to that of the $n = 4$ mode except that the alongshore decay of the coastal jet is now obvious. The values of drag coefficients chosen by Yoshida (1967) are very close to those of the $n = 6$ mode. Thus, the horizontal structure of his upper layer flow looks very much like that of the $n = 4$ or the $n = 7$ mode.

The dynamics of the f-plane model are essentially the same as those for $\beta \neq 0$. High-order modes ($n > 6$) of the f-plane model also tend toward the two-dimensional balance, (32). The similarity between figures 8 and 4*b* is entirely due to the fact that the high-order modes of each model have the same horizontal structure. The low-order modes ($n < 6$) do not tend toward Sverdrup balance. Instead, they tend toward the inviscid balance, (33), with the replacement $k = \sigma^{-\frac{1}{2}}\alpha$. Recall that an alongshore current is associated with this balance. The minor differences between figures 8 and 4*b* arise from alongshore jets being associated with the gravest modes in figure 8.

PHILOSOPHICAL TRANSACTIONS OF THE ROYAL SOCIETY A MATHEMATICAL, PHYSICAL & ENGINEERING SCIENCES

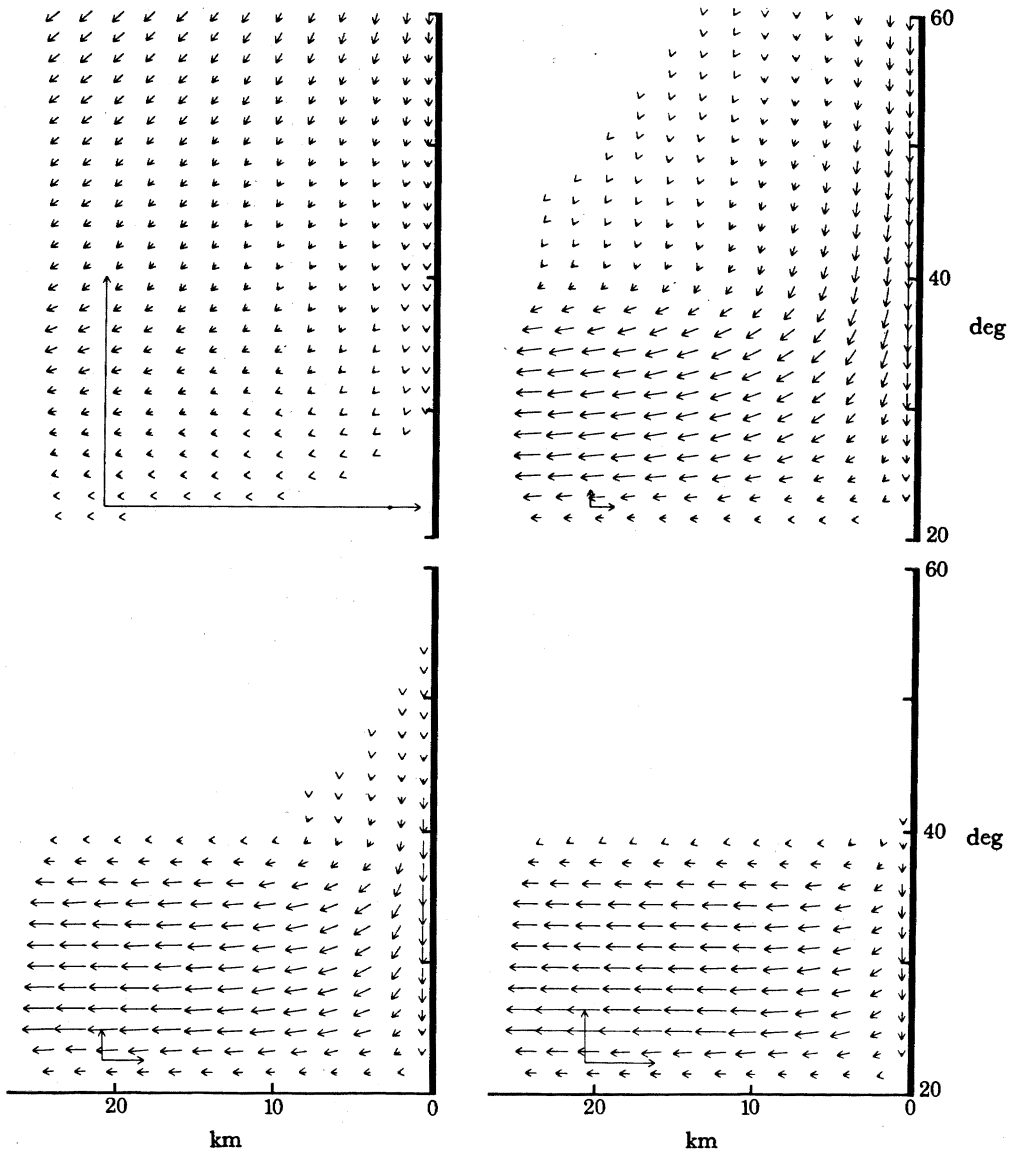

FIGURE 12. The surface velocity fields, due to the $n = 1$ mode (upper left panel), the $n = 4$ mode (upper right panel), the $n = 7$ mode (lower left panel), and the $n = 10$ mode (lower right panel). Calibration vectors are 10 cm/s and 0.1 cm/s in the vertical and horizontal directions, respectively. The $n = 1$ mode is very nearly in Sverdrup balance defined by (34); currents are very weak. The $n = 10$ mode is essentially in two-dimensional balance, defined by (32); the solution is confined to the region of the wind band. The $n = 4$ and $n = 7$ modes have aspects of both balances. The intermediate modes of the model contribute most strongly to the total flow field.

6. SUMMARY AND DISCUSSION

This paper investigates the wind-driven response of the coastal ocean. A model is forced by a steady, equatorward band of wind confined between 20° and 40° N. The eastern ocean boundary is represented by a single vertical barrier. Solutions develop a realistic coastal current structure. Beneath the surface equatorward drift there is a poleward-flowing Coastal Undercurrent with width, thickness and magnitude that compare favourably with those observed. Isopycnals slope sharply upward toward the coast above the Undercurrent and slope weakly downward below.

There is a divergence of surface water from the coast, convergence at and above the core of the Undercurrent, strong upwelling above the current core, and weaker downwelling below. The dynamic height of the sea surface slopes downward from 20° to 38° N and then gradually increases farther poleward. The associated poleward pressure gradient field weakens markedly with depth, becoming weakly equatorward slightly below the core of the Undercurrent.

With the assumptions that $\sigma = 1$ and $\nu_h = \kappa_h = 0$, the response of the model depends on two parameters, $\rho_b(z)$ and ν. The response varies weakly with the shape of the pycnocline beneath the mixed layer, and so also with the magnitude of mixing in the deep ocean. The amplitude of mixing near the core of the Undercurrent does affect the response but less than might be expected. For example, when ν_{min} decreases by two orders of magnitude, the maximum speed of the Undercurrent increases only by a factor of 17. The thickness of the mixed layer influences the speed of the surface equatorward drift, but influences other properties of the flow hardly at all.

The expansion of the solution into vertical normal modes provides a very useful way of discussing the dynamics of the model. The effects of vertical mixing on the low-order modes are small. These modes very nearly adjust to Sverdrup balance. For winds without curl this balance is a state of rest in which an alongshore pressure gradient balances the wind. The radiation of coastal Kelvin and Rossby waves is an essential process in the adjustment of a mode to Sverdrup balance. The effects of vertical mixing dominate the dynamics of the high-order modes, and these modes are very nearly in two-dimensional balance. They add up to generate a transverse circulation pattern characteristic of coastal upwelling. The intermediate modes contribute the most to the alongshore flow. The depth and width scales of the Coastal Undercurrent are therefore set by these modes.

The model is limited in several important ways. It cannot generate any sea surface temperature variations. The model lacks a realistic continental shelf. Finally, nonlinear terms are ignored everywhere, but they are not always small. For example, a consistency check (with the aid of figure 4*d*) shows that the term wv_z is often of the same order of magnitude as the term $(\nu v_z)_z$ in the upwelling corner. Nevertheless, the most important result of this paper is that a simple, stratified, linear model can reproduce the dominant observed features of the Coastal Undercurrent remarkably well, and this agreement suggests that the model contains much of the essential dynamics of the phenomenon.

This research was sponsored by the National Science Foundation under grant no. OCE76-00551 through NORPAX, and by the Office of Naval Research under contract no. N00014-C-75-0165. The author is indebted to Pijush Kundu, whose knowledge of coastal oceanography was an invaluable aid during the course of this study. The efforts of Linda Pugh Fann, Judy Michau and Jan Witte, who helped prepare the manuscript for publication, are greatly appreciated.

Appendix

In this appendix the effects of the horizontal mixing of heat and momentum are retained in the ocean model. The solution of (11) proceeds in a manner very similar to that of section 3 and is only slightly more algebraically complicated. Since the system of equations is now of higher order in x, an additional boundary condition is required at the eastern boundary. A common choice is

$$v_n = 0 \quad \text{at} \quad x = 0, \tag{A 1}$$

and that condition is adopted here.

Again, the wind field is restricted to the form (14), and the alongshore velocity field is assumed to be in geostrophic balance. In addition, since the alongshore scale of the wind stress is large, the operator ∇^2 is replaced with ∂_{xx}. In that case, the first three equations of (11) can be rewritten

$$\left.\begin{aligned} v_n &= \frac{p_{nx}}{f}, \\ u_n &= \frac{G}{f} - \frac{p_{ny}}{f} - \frac{\omega}{f^2} p_{nx} + \frac{\nu_h}{f^2} p_{nxxx}, \\ \nu_h p_{nxxxx} - \omega p_{nxx} - \frac{\nu_h}{\sigma_h}\alpha^2 p_{nxx} - \beta p_{nx} + \frac{\omega}{\sigma}\alpha^2 p_n &= 0, \end{aligned}\right\} \tag{A 2}$$

where $\sigma_h = \nu_h/\kappa_h$ is the horizontal Prandtl number.

In the unbounded ocean the solution to (A 2) is still Ekman flow, (18). Boundary solutions have the form

$$p_n'' = P_1(y)\, e^{k_1(y)x} + P_2(y)\, e^{k_2(y)x} \tag{A 3a}$$

and

$$\left.\begin{aligned} v_n'' &= \frac{1}{f}\left(k_1 P_1 e^{k_1 x} + k_2 P_2 e^{k_2 x}\right), \\ u_n'' &= -\frac{1}{f}\sum_{j=1}^{2}\left(\partial_y + \frac{\omega k_j}{f} - \frac{\nu_h}{f} k_j^3\right) P_j e^{k_j x}, \end{aligned}\right\} \tag{A 3b}$$

where $P_1(y)$ and $P_2(y)$ are, as yet, unspecified functions. The values of $k_1(y)$ and $k_2(y)$ are determined by the third equation of (A 2) to be two of the four roots of

$$\nu_h k^4 - \omega k^2 - (\nu_h/\sigma_h)\,\alpha^2 k^2 - \beta k + (\omega/\sigma)\,\alpha^2 = 0, \tag{A 4}$$

and to satisfy (16 *b*) they are the roots that decay to the west. Since (A 4) is a quartic its roots can be found in closed form just as for a quadratic; so, the evaluation of the roots on a computer is easy.

The imposition of the boundary conditions (A 1) and (16 *a*) results in a coupled pair of equations for P_1 and P_2,

$$\left.\begin{aligned} k_1 P_1 + k_2 P_2 &= 0, \\ (P_1 + P_2)_y - (\nu_h/f)\,(k_1^3 P_1 + k_2^3 P_2) &= G. \end{aligned}\right\} \tag{A 5}$$

Solving for a differential equation in P_1 alone gives

$$[\gamma P_1]_y + (\nu_h/f)\, k_1 k_2 (k_1 + k_2)\,[\gamma P_1] = G, \tag{A 6}$$

where

$$\gamma = 1 - k_1/k_2. \tag{A 7}$$

The solution for γP_1 is

$$\gamma P_1 = e^{-\Lambda}\int_{y_0}^{y} e^{\Lambda}\, Y(y)\, dy, \tag{A 8}$$

where y_0 is any position that lies equatorward of the wind band, and

$$\Lambda = \int^{y} \frac{\nu_h}{f} k_1 k_2 (k_1 + k_2)\, dy. \tag{A 9}$$

The choice of lower limit in (A 8) ensures that (16 *b*) is satisfied.

With the specification of P_1, P_2 is also determined. So, the fields u_n'', v_n'' and p_n'' are known. The p_n-field, the sum of p_n' and p_n'', is therefore

$$p_n'' = \tau_{0n}\frac{k_2 e^{k_1 x} - k_1 e^{k_2 x}}{k_2 - k_1} e^{-\Lambda}\int_{y_0}^{y} e^{\Lambda}\, Y dy. \tag{A 10}$$

The other fields can be readily found with the aid of (A 2).

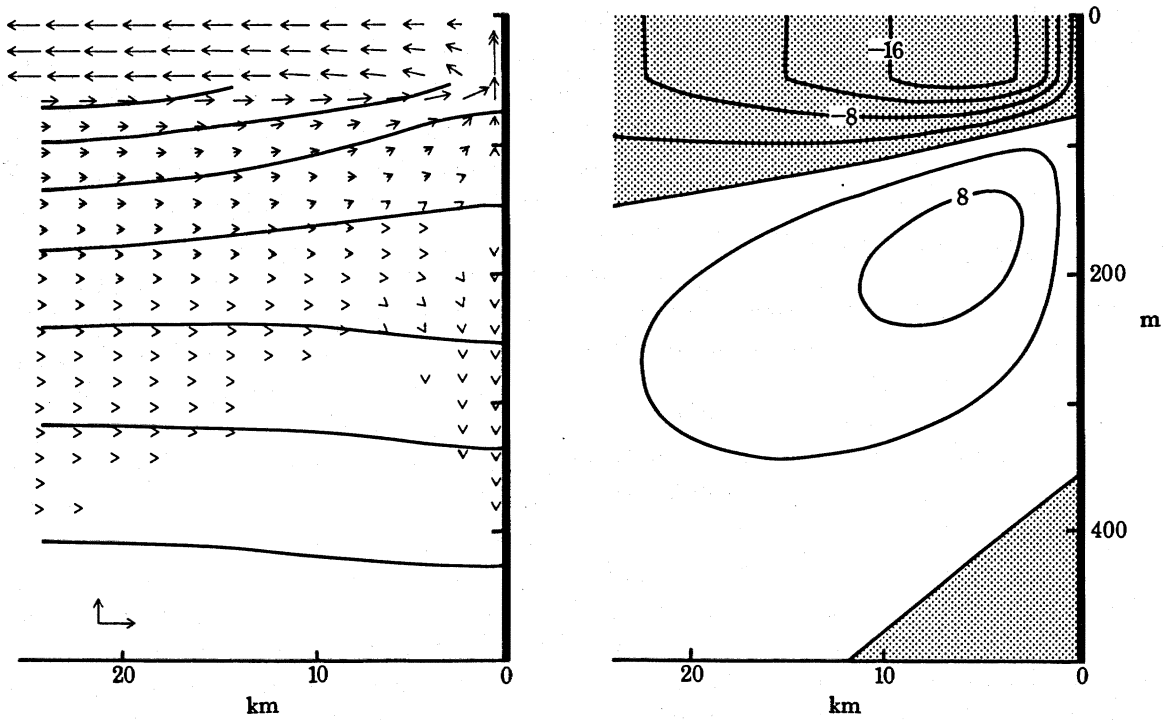

FIGURE 13. Vertical section of a flow field that includes the effect of horizontal mixing, showing transverse circulation and isopycnal structure (left panel) as well as alongshore current (right panel) along section 2 of figure 3. Contour intervals and calibration vectors are the same as in figure 4*a*. The alongshore flow field is weakened by horizontal mixing, and necessarily has offshore maxima.

Figure 13 shows the model response, including effects of horizontal mixing, that is otherwise comparable with figure 4*b*. The value of the horizontal eddy viscosity is $\nu_h = 10^5$ cm/s, and the horizontal Prandtl number is $\sigma_h = 1$. The flow fields are very similar. The major differences are that in figure 13 the alongshore currents are weaker and necessarily have offshore maxima. So, the introduction of horizontal mixing into the ocean model does alter the amplitude and structure of the Coastal Undercurrent, but not significantly. Horizontal mixing processes are evidently not an essential element of the dynamics of the Coastal Undercurrent.

The horizontal structure and dynamics of (A 10) vary with mode number very similarly to those of (25). The alongshore decay scale is l^{-1}, where

$$l \equiv -e^{\Lambda}(e^{-\Lambda})_y = \Lambda_y = (\nu_h/f)\, k_1 k_2 (k_1 + k_2). \tag{A 11}$$

The offshore decay scales are measured by k_1^{-1} and k_2^{-1}. For low-order modes k_1 and k_2 are approximately

$$k_1 = (\omega/\beta)\,(\alpha^2/\sigma), \quad k_2 = (\beta/\nu_h)^{\frac{1}{3}}. \tag{A 12}$$

For high-order modes, and for unit Prandtl number, they are

$$k_1 = \alpha, \quad k_2 = (\omega/\nu_h)^{\frac{1}{3}}. \tag{A 13}$$

The quantities l, k_1 and k_2, are all monotonically increasing functions of mode number, and so the solutions are increasingly coastally trapped and more latitudinally confined to the region of the wind band. The equality $l\Delta y = 1$ again marks a transition in the dynamics of the solution. When $l\Delta y \ll 1$ the solution is very nearly in inviscid balance, and when $l\Delta y \gg 1$ the solution is virtually in two-dimensional balance.

Several previous ocean models are quite similar to the one described in this Appendix in that they involve horizontal mixing and find the coastal response as expansions of vertical normal modes. In the Pedlosky (1969) model offshore decay scales have forms equivalent to (A 12), and $l \equiv 0$. So, *all* the modes of his coastal boundary layer behave like the low-order modes of the present model, and there is no transition to two-dimensional dynamics with increasing mode number. His solution is unrealistic in that both the coastal upwelling and the alongshore current have surface singularities. (Pedlosky did not provide any pictures of his solution. However, Barcilon (1971) did show a schematic representation of an analogous solution; isopycnals all converge to the upwelling corner.) In the Allen (1973) model the offshore decay scales of the steady solution have forms equivalent to (A 13), but solutions necessarily cannot develop alongshore pressure gradients. Consequently, *all* the vertical modes of his coastal boundary layer behave like the high-order modes of the present model, and there is no transition to inviscid dynamics for sufficiently low mode number. Allen's steady solution suffers from the same drawbacks as does the solution of figure 9. The dynamics of the Pedlosky (1974) model are essentially the same as those discussed here. There is an alongshore decay scale associated with each mode that is equivalent to (A 11). Therefore, as in the present model, low-order modes establish alongshore pressure gradients to balance the wind, and high-order modes tend toward a two-dimensional balance where those pressure gradients play no role. It was pointed out in the Introduction that this solution had features that compared favourably with the observed Coastal Undercurrent. Curiously, as the last sentence of his paper suggests, Pedlosky did not feel that his solution was applicable to the phenomenon.

References

Allen, J. S. 1973 Upwelling and coastal jets in a continuously stratified ocean. *J. phys. Oceanogr.* **3**, 245–257.

Allen, J. S. 1980 Models of wind-driven currents on the continental shelf. *A. Rev. Fluid Mech.* **12**, 389–433.

Anderson, D. L. T. & Gill, A. E. 1975 Spin-up of a stratified ocean, with application to upwelling. *Deep Sea Res.* **22**, 583–596.

Barcilon, V. 1971 A simple model of the thermocline in a bounded ocean. *J. phys. Oceanogr.* **1**, 7–11.

Brink, K. H., Allen, J. S. & Smith, R. L. 1978 A study of low-frequency fluctuations near the Peru coast. *J. phys. Oceanogr.* **8**, 1025–1041.

Brockmann, C., Fahrbach, E., Huyer, A. & Smith, R. L. 1980 The poleward Undercurrent along the Peru coast: 5°–15 °S. *Deep Sea Res.* **27**, 847–856.

Caldwell, D. R., Dillon, T. M., Brubaker, J. M., Newberger, P. A. & Paulson, C. A. 1980 The scaling of vertical temperature gradient spectra. *J. geophys. Res.* **84**, 1917–1924.

Charney, J. G. 1955 The generation of oceanic currents by wind. *J. mar. Res.* **14**, 477–498.

Chelton, D. B. 1980 Low frequency sea level variability along the west coast of North America (212 pp.). Ph.D. thesis, University of California at San Diego.

Defant, A. 1941 Die absolute Topographie des physikalischen Meeresniveaus und der Druckflächen im Atlantischen Ozean. *Wiss. Ergebn. dt. atlant. Exped.* '*Meteor*' **6**, 2.

Durance, J. A. & Johnson, J. A. 1970 East coast ocean currents. *J. Fluid Mech.* **44**, 161–172.

Fjeldstad, J. E. 1963 Internal waves of tide origin. *Geofys. Publr.* **25**, 1–73.

Garvine, R. W. 1971 A simple model of coastal upwelling dynamics. *J. phys. Oceanogr.* **4**, 169–179.

Gill, A. E. & Clarke, A. J. 1974 Wind-induced upwelling, coastal currents and sea-level changes. *Deep Sea Res.* **21**, 325–345.

Hickey, B. M. 1979 The California Current system – hypotheses and facts. *Prog. Oceanogr.* **8**, 191–279.

Huyer, A. 1976 A comparison of upwelling events in two locations: Oregon and northwest Africa. *J. mar. Res.* **34**, 531–546.

Lighthill, M. J. 1969 Dynamic response of the Indian Ocean to the onset of the Southwest Monsoon. *Phil. Trans. R. Soc. Lond.* A **265**, 45–93.

Lilly, D. K., Waco, D. E. & Adelfang, S. I. 1974 Stratospheric mixing estimated from high-altitude turbulence measurements. *J. appl. Met.* **13**, 488–493.

PHILOSOPHICAL TRANSACTIONS OF THE ROYAL SOCIETY A MATHEMATICAL, PHYSICAL & ENGINEERING SCIENCES

McCreary, J. P. 1976 Eastern tropical ocean response to changing wind systems: with application to El Niño. *J. phys. Oceanogr.* **6**, 632–645.

McCreary, J. P. 1977 Eastern ocean response to changing wind systems. Ph.D. thesis (156 pp.), University of California at San Diego.

McCreary, J. P. 1978 Eastern ocean response to changing wind systems. In *Review papers of equatorial oceanography: FINE workshop proceedings* (held in La Jolla, California). Fort Lauderdale, Florida: Nova University/NYIT Press.

McCreary, J. P. 1981 A linear stratified ocean model of the Equatorial Undercurrent. *Phil. Trans. R. Soc. Lond.* A **298**, 603–635.

Mittelstadt, E. 1978 Physical oceanography of coastal upwelling regions with special reference to Northwest Africa. Paper presented at Symposium on the Canary Current: upwelling and living resources (held in Las Palmas, Gran Canaria).

Mittelstadt, E., Pillsbury, D. & Smith, R. L. 1975 Flow patterns in the North-west African upwelling area. Results of measurements along 21° 40′ N during February–April 1974. JOINT-1. *Dt. hydrogr. Z.* **28**, 145–167.

Moore, D. W. & Philander, S. G. H. 1978 Modelling of the tropical ocean circulation. In *The sea*, vol. 6, pp. 319–361. New York: Wiley Interscience.

Mork, M. 1972 *On the time-dependent motion induced by wind and atmospheric pressure in a continuously stratified ocean of varying depth* (43 pp.). Geophys. Inst. Div. A, Phys. Oceanogr., University of Bergen, Norway.

Nelson, C. S. 1976 Wind stress and wind stress curl over the California coast. M.S. thesis, Naval Postgraduate School, Monterey, California (136 pp.).

O'Brien, J. J. & Hurlburt, H. E. 1972 A numerical model of coastal upwelling. *J. phys. Oceanogr.* **2**, 14–26.

O'Brien, J. J., Clancy, R. M., Clarke, A. J., Crepon, M., Ellsburg, R., Grammelsrod, T., MacVean, M., Röed, L. P. & Thompson, J. D. 1977 In *Modelling and predicting the upper layers of the ocean*, pp. 178–228. New York: Pergamon Press.

Pedlosky, J. 1968 An overlooked aspect of the wind-driven ocean circulation. *J. Fluid Mech.* **32**, 809–821.

Pedlosky, J. 1969 Linear theory of the circulation of a stratified ocean. *J. Fluid Mech.* **35**, 185–205.

Pedlosky, J. 1974 On coastal jets and upwelling in bounded basins. *J. phys. Oceanogr.* **4**, 3–18.

Reid, J. L. & Mantyla, A. W. 1976 The effect of geostrophic flow upon coastal sea elevations in the northern North Pacific Ocean. *J. geophys. Res.* 3100–3110.

Sverdrup, H. U. 1947 Wind-driven currents in a baroclinic ocean: with application to the equatorial currents of the Eastern Pacific. *Proc. Natn. Acad. Sci. U.S.A.* **33**, 318–326.

Turner, J. S. 1973 *Buoyancy effects in fluids*. Cambridge University Press.

Veronis, G. 1973 Large-scale ocean circulation. In *Advances in applied mechanics*, vol. 13. New York: Academic Press.

Wooster, W. S. & Gilmartin, M. 1961 The Peru-Chile Undercurrent. *J. mar. Res.*, **19**, 97–122.

Wooster, W. S. & Reid, J. L. 1963 Eastern boundary currents. In *The sea*, vol. 2, pp. 253–280. New York: John Wiley and Sons.

Wooster, W. S. & Jones, J. H. 1970 California Undercurrent off Baja California. *J. mar. Res.* **28**, 235–250.

Wyllie, J. G. 1966 Geostrophic flow of the California Current at the surface and at 200 meters. *California Cooperative Oceanic Fisheries Investigations, Atlas no.* 4 (288 pp.).

Yoshida, K. 1955 Coastal upwelling off the California coast. *Records oceanogr. Wks Japan* **15**, 1–13.

Yoshida, K. 1967 Circulation in the eastern tropical ocean with special references to upwelling and undercurrents. *Jap. J. Geophys.* **4**, 1–75.

PHILOSOPHICAL TRANSACTIONS OF THE ROYAL SOCIETY A MATHEMATICAL, PHYSICAL & ENGINEERING SCIENCES